Strong Metal-support Interactions in Photocatalysis: Fundamentals and Design Methods

Vien-duong Quach, Robert Wojcieszak, Mohamed Nawfal Ghazzal

ACES Asian Chemical Editorial Society

doi.org/10.1002/cnma.202300329

CHEMNANOMAT
Review

www.chemnanomat.org

Strong Metal-support Interactions in Photocatalysis: Fundamentals and Design Methods

Vien-Duong Quach,[a] Robert Wojcieszak,[b] and Mohamed Nawfal Ghazzal*[a]

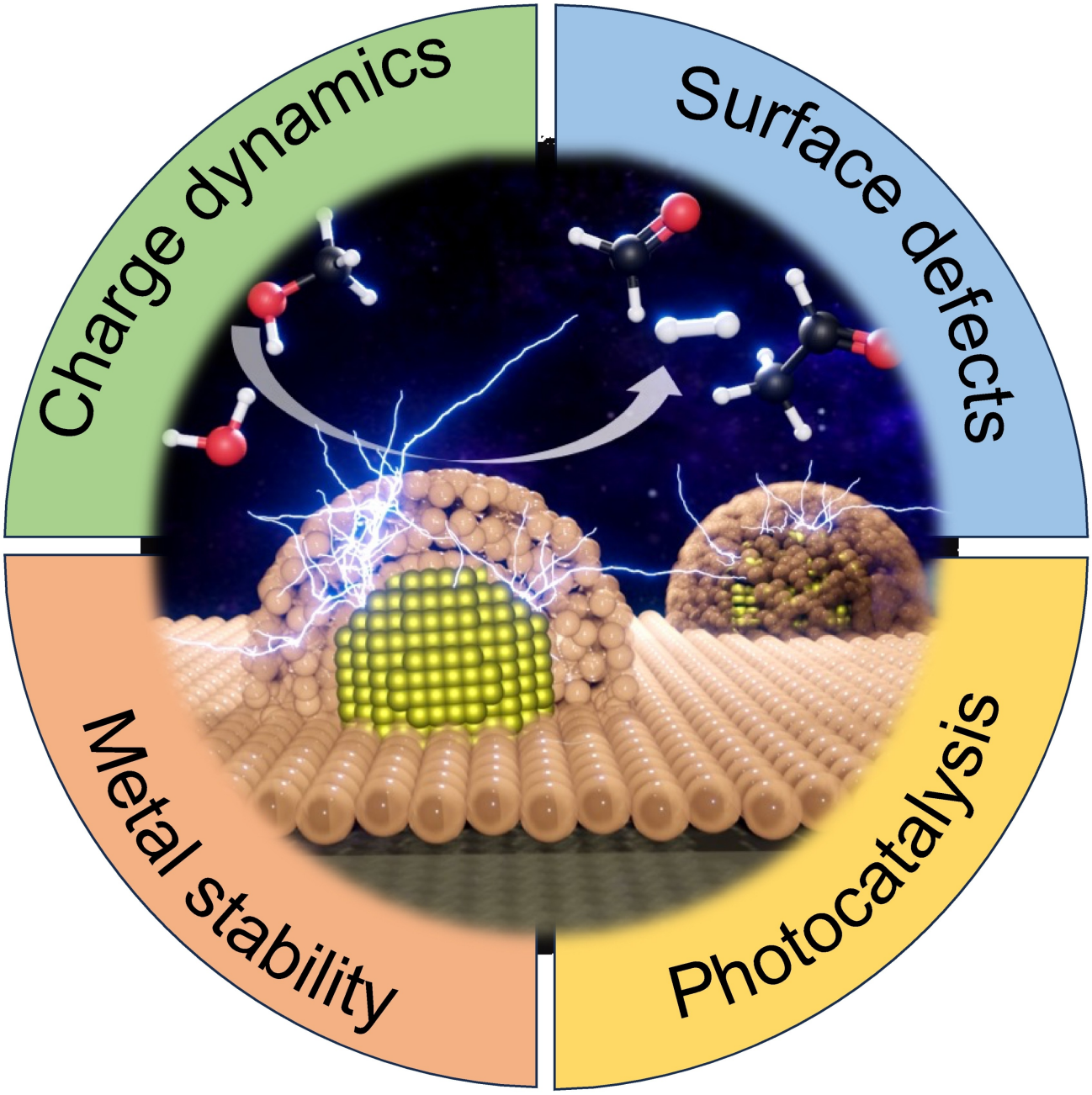

Engineering the composition and geometry of metallic sites has become a popular manner to boost reaction rate and control reaction selectivity in heterogeneous catalysis. Many studies have been devoted to enhancing the stability of metallic nanoparticles during catalytic reactions by dispersion on metal oxide supports such as TiO_2, CeO_2 or Nb_2O_5. These supports not only modulate electronic properties and dispersion/stabilization of metallic nanoparticle but also influence catalytic selectivity, resulting in the so-called "strong metal-support interaction" (SMSI). In this minireview, we outlined the discovery and fundamentals of SMSI, as well as its extensive development over years. In addition, we summarized recent approaches developed to induce the construction of SMSI between different metal nanoparticles and metal oxide supports. Associated characterization microscopic and spectroscopic techniques were emphasized. Despite being a prevalent concept in catalysis, the number of studies on SMSI in heterogeneous photocatalysis has been even in limitation. Herein, we highlighted the beneficial effects of SMSI on boosting photocatalytic activity for CO_2 reduction and H_2 evolution reactions. In general, despite some controversial aspects of the SMSI, this concept offers wide opportunities ahead and encourages researchers to rethink the local active site localization and photocatalyst design.

1. Introduction

Heterogeneous photocatalysts mediated by metallic nanoparticles, especially plasmonic metals, have shown superior properties and higher efficiency in the solar-to-energy conversion yield.[1–6] The metallic nanoparticles have been reported for boosting the photocatalytic efficiency of variable reactions, such as CO_2 reduction,[7–10] CO_2 methanation,[11–13] hydrogeneration,[14–16] and alcohol conversion.[17,18] However, further investigations are expected to understand the effect of photocatalyst design, the intrinsic activities of metallic nanoparticles, and the benefits of constructing strong interaction with reducible oxides as supports on the photocatalytic performance. Particularly, strong metal-support interaction (SMSI) between single metal atoms and semiconductors has become a central topic that much research involved to pinpoint SMSI effects on catalytic activities. This review aims to summarize several key factors of strong metal-support interaction, resulting in a brief and easily approachable view in this field.

The term "strong metal-support interaction" (SMSI) was first launched in 1978 by Tauster *et al.*[19] in order to explain the change in chemisorption properties of VIIIB group metals (Ru, Rh, Pd, Os, Ir, Pt) supported on TiO_2 when increasing reduction temperature. The research group used impregnation of metal salt solutions on commercial TiO_2 (P25 Degussa and Cab-O-Ti Cabot) to prepare catalysts. They recorded considerable H_2 and CO uptakes on catalysts at low reduction temperature (200 °C), demonstrating high dispersion of metal clusters. As the reduction temperature was increased to 500 °C, the CO adsorption was found to decrease dramatically to near zero. The agglomeration of metal clusters due to the rise in temperature treatment and poisoning by impurities was found not inducing such a depletion in H_2 and CO chemisorption. Thus, the encapsulation of metal particles occurring under H_2 flow and at 500 °C was considered, despite the reversibility of the chemisorption. Indeed, metal particles should be accessible to gaseous molecules to experience reversible adsorption/desorption.[20]

The mechanism of SMSI encapsulation generally leans on the reduction of metal oxide support by H_2 at elevated temperature. It is well-accepted that the dissociation of H_2 molecules into H atoms on metal nanoparticle surface is the key driving force of reducing metal oxides.[21] The high temperature could promote redox reactions between metal nanoparticles and metal oxide supports, leading to changes in the oxidation state of metals.[22,23] Then, reduced metal cations are formed, which modulate Fermi levels of metal oxides, resulting in charge transfer as well as redistribution of electron density at the metal-support interface. The charge redistribution at the interface is the key of the construction of mixed oxides[24,25] and alloys,[25–27] which grow gradually and migrate onto metal nanoparticles, thus illustrating an overlayer of reduced metal oxide supports.[28]

In order to explain the unique chemisorption properties of the samples, Tauster *et al.*[19] suggested that the change in the chemical interactions between the noble metals and the support at surface, the so-called strong metal-support interaction (SMSI), is the main phenomenon modifying the chemisorption of CO. In particular, fully electron occupied *"d"* orbitals of noble metals are likely to overlap with vacant *"d"* orbitals of $Ti^{[4+]}$ cations, resulting in metal-metal bonding, under reducing conditions. The interaction between the *"d"* orbitals of donor-acceptor thermodynamically favourable to the formation of intermetallic bonds (Ti-M_3), and presumably induces a change in the sorption properties at the surface of metal nanoparticles. The SMSI effect was expanded exclusively to reducible binary oxides including MnO_2, V_2O_5, Nb_2O_5 even when activation temperature was lower than 500 °C.[29] The suppression of hydrogen and carbon monoxide were not recorded with SiO_2, Al_2O_3, MgO, ZrO_2, Sc_2O_3, HfO_2, Y_2O_3. In other words, these non-reducible oxides typically exhibit no SMSI behaviour. The key solid-state transformations in reactive

[a] *Mr. V.-D. Quach, Dr. M. N. Ghazzal*
Insitut de Chimie Physique (ICP)
UMR 8000 CNRS, Université Paris-Saclay
F-91400, Orsay (France)
E-mail: mohamed-nawfal.ghazzal@universite-paris-saclay.fr
[b] *Dr. R. Wojcieszak*
Unité de Catalyse et Chimie du Solide (UCCS)
UMR 8181 CNRS, Université de Lille
F-59000, Lille (France)

systems leading to the construction of strong metal-support interaction was the migration of reducible metal oxide support fully covering metal nanoparticles.[20,30] The metal oxide migration during the reduction process induces morphology change of metal particles. Large metal particles break up into smaller raftlike configurations that were fringed with the reduced surface of TiO_2. In the meantime, the surface reduction of the support incentivized oxygen vacancies generation that would facilitate the proximity between metal atoms and reduced cations. The generation of oxygen vacancies at the metal/metal oxide overlayer was an indicative sign of the strong metal-support interaction in which titanium ions are the key. Several studies demonstrated chemical bonds between some VIIIB group metals, including Ni, Pt, Pd, Rh, and $Ti^{[3+]}$ cations. The TiO_2 overlayer was found to have variable effect regarding the main catalytic reaction. For instance, it was observed that the construction of SMSI using titanium oxide overlayer modify the chemisorption capacities towards H_2 and CO, as well as the catalytic activity in hydrogenolysis and dehydrogenation.[31] However, encapsulation of metal particles such as Pt in TiO_2 or Nb_2O_5 was reported boosting the Fischer-Tropsch reaction rate of CO and H_2 to produce methane and other hydrocarbon.[32] While the construction of SMSI was restricted to group VIII metals, recent developments have been conducted and led to the extension of SMSI to other metallic nanoparticles. Over the past years, plenty of studies reported "SMSI" construction or effect to describe a change in the charge transfer, catalytic activity or molecules adsorption invoking the role of the metal/support interface, even when an encapsulation layer is not observed. In this review, we will mainly focus on variable strategies used for the construction of SMSI using validated metal oxide overlayer covering metallic nanoparticles. We discuss herein the SMSI phenomenon on different metallic nanoparticles and the strategies to be applied to enhance the SMSI on various catalytic systems.

2. SMSIs regarding different metallic nanoparticles

2.1. SMSIs to platinum nanoparticles

Platinum nanoparticles might be one of the pioneering and widely-studied objects in the field of strong metal-support interaction catalysts.[19,33,34] Pt nanoparticles (larger size) are more likely to undergo SMSI encapsulation than Pt single atoms (smaller size) because of a difference in electronic structures. Belton and co-workers performed controlled coverage of Pt with thin titanium oxide and studied the electronic structures and charge transfers under ultrahigh-vacuum.[35] Even though the encapsulation of Pt nanoparticles has been investigated on different reducible oxides; such as Fe_3O_4,[36,37] TiO_2,[38,39] WO_3,[39,40] CeO_2,[41–43] etc., titanium dioxide remains by far the most studied support. However, the crystalline structure and receding of TiO_x overlayers during catalytic reaction deteriorate the catalytic performance of support metal co-catalysts. The influence of annealing temperature and metal nanoparticle size on the encapsulation of Pt nanoparticles by support overlayers have been also studied. The migration of TiO_x ($1 \leq x \leq 3$) took place during encapsula-

Vien-Duong Quach is currently a Ph.D. candidate in Material Chemistry at Institute of Physical Chemistry, CNRS UMR 8000, Université Paris-Saclay, France. He conducted an undergraduate study on Material Chemistry at Vietnam National University, Hanoi. He was then a scholar in the Erasmus Mundus Joint Master SERP + program (surface, electro, radiation, photochemistry) whereby he received double M.Sc. degrees in Physical Chemistry and Materials Science from Université Paris-Saclay (France) and Università di Genova (Italy). His work centers on strong metal support interaction-simulated core@shell nanostructures mediated by metallic nanoparticles and their applications on photocatalysis and photoelectrocatalysis.

Robert Wojcieszak is a senior researcher at the CNRS in Lille, France. He obtained his Ph.D. in Molecular Chemistry from Henri Poincare University in 2006 and subsequently held a Postdoctoral Fellowship in the IMCN at the Catholic University of Louvain, Belgium. Then, he was a FAPESP fellow at the University of São Paulo, Brazil. His research interests cover materials science and catalytic materials design. Especially he is working on the development of new advanced catalysts for biomass transformation especially for the oxidation and hydrogenation of bio-based compounds and hybrid catalysis. He is the coordinator of the CatBioInnov group at Centrale Lille, France.

Mohamed Nawfal Ghazzal is an Associate Professor at the Université Paris-Saclay. He is now investigating strategies aiming at improving the light harvesting ability, the stability and designing photoactive material, such as core-shell, strong metal-support interactions, perovskites, graphdiyne for photocatalytic applications.

tion process at a temperature above 150 °C even in the absence of H_2 as a reducing atmosphere,[44–47] while a sintering process would dominate the encapsulation process when annealing temperature is above 300 °C.[48,49] It was also reported that Pt nanoparticles and Pt single atoms could trigger SMSI with TiO_2 support but at different annealing temperatures.[50]

Wu *et al.*[51] studied the sensitivity of SMSI to the size of Pt particles supported on rutile TiO_2 by means of spectroscopic techniques. Pt nanoparticles are dominant at thicker coverage of 0.41 and 2.5 monolayer (ML), while Pt coverage of 0.06 ML generates both Pt clusters and Pt nanoparticles. Besides, 0.41 and 2.5 ML-Pt/TiO_2 showed the entire encapsulation of Pt nanoparticles into TiO_{2-x} overlayers evidencing Pt-TiO_2 SMSI, and Pt nanoparticles on 0.06 ML-Pt/TiO_2 as well. However, Pt clusters do not exhibit the possible construction of SMSI. Moreover, no aggregation of Pt clusters into Pt nanoparticles was recorded on the sample after annealing at 727 °C. This indicated that high thermal stability of Pt clusters was due to the nucleation at surface oxygen vacancy sites of TiO_2 surface. The research group suggested that the influence of Pt particle size on SMSI might be related to their electronic structures. The charge transfer in Pt-TiO_2 SMSI typically operates from Pt to Ti[30] through Pt-Ti-O linkage. Indeed, Pt clusters with depleted charge in the "*d*" orbital and contracted lattice might be less capable of transferring charge to Ti, whereas larger Pt nanoparticles are more likely to form Pt-Ti-O interface and trigger the charge transfer through the construction of SMSI. The influences of particle size on SMSI, particularly Pt nanoparticles supported over Fe_3O_4,[36] were also studied. The CO oxidation reaction, involving chemisorption of CO and O_2, emphasized an important contribution of Langmuir-Hinshelwood mechanism between the two reactants on larger Pt nanoparticles (Figure 1a). Besides, the partial coverage of TiO_x would stabilize Pt nanoparticles against sintering process at high annealing temperature.

Through a study on Pt-CeO_2 catalyst at microscopic level, Vayssilov *et al.*[26] identified two experimental hallmarks of SMSI: 1)- electron transfer from Pt NPs to CeO_2 support, and 2)- oxygen transfer from CeO_2 to Pt NPs. The electron transfer takes place on both surface and bulk of CeO_2, while the oxygen transfer would be exclusive at the interface Pt-CeO_2. In this study, the highest occupied molecular orbital (HOMO) and the lowest unoccupied molecular orbital (LUMO) in CeO_2 nanoparticles was regulated to CeO_2 (111) surface that HOMO and LUMO predominantly were assigned to O 2p orbitals and Ce 4f orbitals, respectively.[52] Introduction of Pt clusters fills the whole band gap HOMO-LUMO, as illustrated in Figure 1b. Because the highest occupied levels of Pt are in the vicinity of empty Ce 4f (LUMO), the author inferred electron transfer from Pt metal clusters to Ce to form Ce^{3+} ions. The charge transfer would accompany with partial reduction of Pt clusters as well. Considering oxygen vacancy formation, theoretical calculation predicted Ce^{3+} ions deriving from oxygen detachment are detected exclusively at the Pt-CeO_2 interface. The changes in the oxidation state of CeO_2 due to molecular interactions, involving Ce^{3+} ($4d^{10}4f^1$) and Ce^{4+} ($4d^{10}4f^0$), were

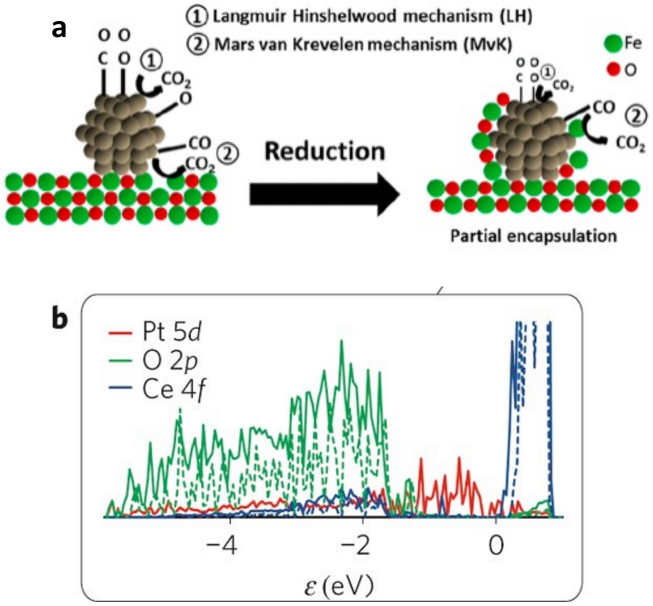

Figure 1. (a) Strong metal-support interactions between Pt nanoparticles and Fe_3O_4 support. Reprinted with permission from.[36] Copyright American Chemical Society, 2020. (b) Density-of-states plot for the bare nanoparticle $Ce_{40}O_{80}$ (dashed lines) and the nanoparticle system $Pt_8/Ce_{40}O_{80}$ (solid lines). Reprinted with permission from.[26] Copyright Springer Nature, 2011.

investigated by resonant photoelectron spectroscopy (RPES) at room temperature and then during annealing. The deposition of Pt on CeO_2 film axhibited the formation of Ce^{3+} centres, which was not detectable before. The result evidences that Ce^{3+} are generated on surface and in the region of Pt clusters. When elevating temperature over 300 °C, Ce^{3+} concentration showed an increase. This is attributed to reverse spillover of oxygen from CeO_2 to Pt NPs, as expected through DFT calculation.

Baker *et al.*[21] demonstrated the role of Pt in dissociating H_2 at 550 °C, which provides H atoms to reduce TiO_2 and form substoichiometric oxide (Ti_4O_7). In order to assess the necessary of H_2 dissociation in the generation of SMSI, the authors examined the behaviour of Ag nanoparticles on TiO_2 support with and without the presence of Pt nanoparticles. The specimen of Ag/TiO_2 outputted only a change in morphology of Ag NPs, including larger size and relatively dense and globular in outlines. Besides, TiO_2 support was in rutile form, no transformation was recorded. This confirmed SMSI interaction does not take place in this case. In contrary, (Ag + Pt)/TiO_2 exhibited remarkable change in the characteristics of these metal NPs. The metal crystallites of Ag became small, very thin, and especially angular in outline compared to the aforementioned globular outlines. With the presence of Pt, the rutile TiO_2 converted to Ti_4O_7, Ag NPs typically exhibited SMSI morphological features when supported on Ti_4O_7. The authors also inferred charge transfer between the reduced support and small Ag NPs through an EPR study that pointed out the formation of Ti^{3+} and partial reduction of Ag^+ to Ag^0 during thermal treatment. In brief, SMSI interaction can be induced

with metals which do not dissociate H_2 if another metal was added to catch the mission, Pt in this specific study.

2.2. Extension of SMSIs to IB group metals

Transition metals having work functions and surface energies exceeding a certain value would be likely to undergo the above-mentioned encapsulation and thus practice SMSIs.[53] Meanwhile, metals outside group VIIIB with lower work functions and surface energies was reported not to be sensitive to SMSI encapsulation.[19] However, over the past decade, research groups pioneered classical SMSI between reducible oxides (TiO_2, ZnO) and IB group metals (such as Au and Ag),[54–58] leading to an extension of studies in SMSI afterward.

Mei et al.[54] reported the agglomeration of TiO_x in the vicinity of Au nanoparticles and the generation of Au/TiO_2 core-shell structures on an account of SMSI. The overlayer of TiO_x over Au probably depends on its loading. The authors inferred the relation between Au/TiO_2 composites with variable Ti loading and photocatalytic H_2 evolution (Figure 2). Particularly, less extent of the Au/TiO_2 core-shell structure would be accompanied by lower number of active sites and hence lower amount of H_2. Indeed, a sample in which the agglomeration of TiO_x was deliberately blocked produced negligible amount of H_2. The results pointed out diffusion-controlled photo-deposition lead to smaller size of Au NPs due to strong metal-support interactions.

Tang *et al.*[56] reported the construction of classical strong metal-support interaction between Au NPs and TiO_2, evidenced by suppression of CO adsorption, electron transfer from oxide support to metal nanoparticles, and gold encapsulation by reduced TiO_2 overlayer at high-temperature reducing environment. In this study, Au NPs were deposited on different polymorphs of titania, including P25 (Degussa), anatase, and rutile, these samples underwent high temperature reduction (HTR) treatment to 500 °C in H_2/He (10% v/v) before being reoxidized at 400 °C in O_2/He (10% v/v). *In situ* diffuse reflectance infrared Fourier transform spectroscopy (DRIFTS, Figure 3a) indicated a band of absorbed CO on metallic Au at 2103 cm^{-1}, the band intensity depleted with elevating reduction temperature and nearly faded after 500 °C. This evidenced the loss of CO adsorption sites due to SMSI encapsulation. Through X-ray photoelectron spectroscopy (XPS), the authors recorded the existence of negative Au surface species during reduction at over 400 °C and their reverse to the metallic state after reoxidation step, observed by a small shift of binding energy from 83.5 eV to 83.1 eV then back to 83.5 eV (Figure 3b). It was attributed to reversible electron transfer between TiO_2 and Au, which reveals the occurrence of SMSI, likewise, TiO_2-supported platinum group metals previously reported. Besides, they highlighted an increase in Ti^{3+} defects from electron paramagnetic resonance (EPR, Figure 3c), which evidenced the reduction of TiO_2 after high-temperature reduction treatments. It emphasized that titania reduction is a key factor in inducing SMSI encapsulation.

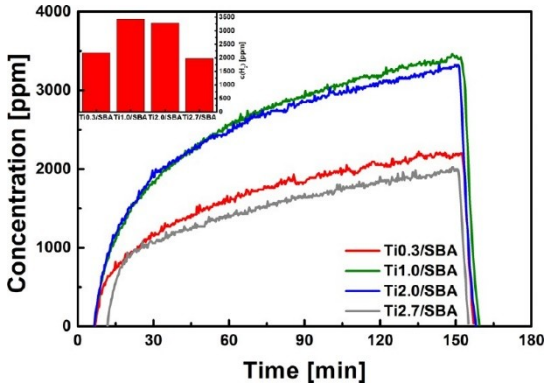

Figure 2. Hydrogen evolution measured during the photodeposition process of Au (0.25 wt.%) on Ti(x)/SBA materials with increasing Ti loading. Reprinted with permission from.[54] Copyright American Chemical Society, 2013.

Among polymorphs of titania oxides, anatase was found to be the most susceptible to encapsulation, while rutile, the most stable phase, is less favourable to SMSI encapsulation. Surprisingly, the SMSI encapsulation of Au occurs not only for TiO_2 but also for Fe_3O_4 and CeO_2 after a reduction treatment at 500 °C, which is much lower than 700 °C for Pt/CeO_2 and Rh/CeO_2.[59,60] Tang *et al.*[56] investigated the SMSI of other IB group metals (such as Cu and Ag) supported over TiO_2. Experimental outputs showed reversible CO adsorption and encapsulation of Ag NPs at 500 °C, indicating classical SMSI between Ag NPs and TiO_2. At the same time, the migration of the metal oxide support over Cu NPs was found difficult, due to a lack of TiO_2 reduction, evidenced by a decrease of Ti^{3+}. The SMSI construction on Cu/TiO_2 required reduction treatment at higher temperatures (above 700 °C). In the contrary to previous studies, which reported the limited application of Au and Ag in catalysis due to their poor thermal stability at high temperatures, classical SMSI in Au/TiO_2 demonstrated its excellent stability toward catalytic CO oxidation and even slow deactivation. The stability was ascribed to metal-promoted oxygen vacancy generated in Au/metal oxide interface.

Zhang *et al.*[61] provided solid experimental evidence that divulged two key factors of inducing strong metal-support interactions on Au/TiO_2 catalyst: 1)- particle size of supported Au NPs and 2)- facets of TiO2 supports. This study focused on Au NPs of 2 nm and 5 nm in size which were separately supported on different TiO_2 supports with different facets, including {100}, {001}, and {101}. The Au/TiO_2 SMSI was induced by high-temperature annealing treatment. The authors adjusted the size of Au NPs by changing the annealing environment.[46] They obtained Au NPs of 5 nm after doing treatment in air (oxidative O_2) while the size of Au NPs was smaller, around 2 nm, when replacing air by H_2 reductive atmosphere. In fact, O_2 in air would strengthen Ostwald ripening of metal NPs during annealing. The suppression of CO adsorption, investigated by in situ DRIFT spectroscopy, signifies the modification of surface structure after the annealing treatment (Figure 3d). 5 nm Au/TiO_2 samples recorded no CO adsorption, while much weaker peaks of CO adsorption still appeared in DRIFT spectra of 2 nm Au/TiO_2

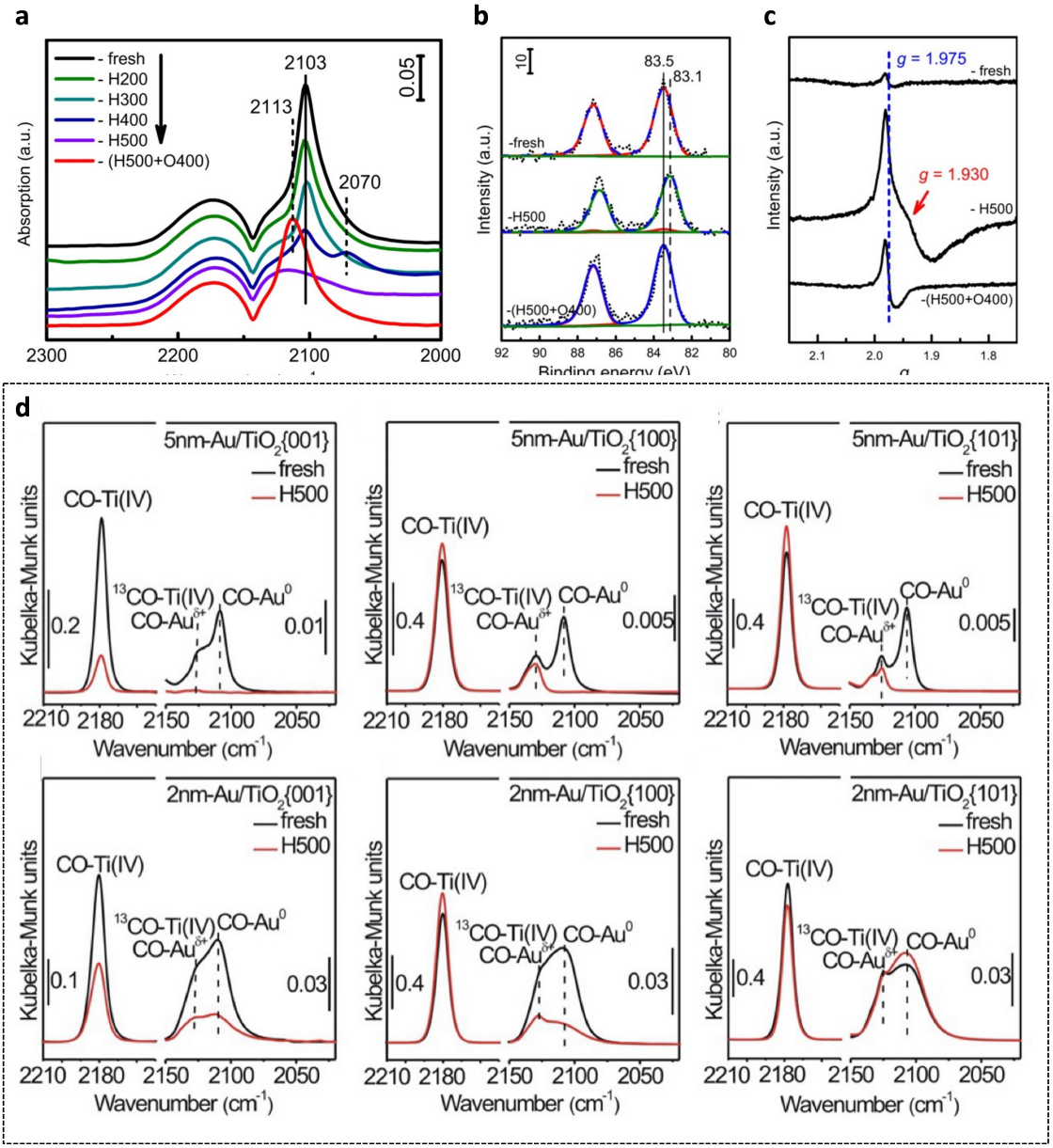

Figure 3. (a) In situ DRIFT spectra of CO adsorption over Au/TiO_2 fresh and those reduced at elevated temperature from 200 °C to 500 °C (H200 to H500) before being reoxidized at 400 °C (H500 + O400). (b) Negatively shifted Au 4f XPS peak of Au/TiO_2 high-temperature reduction at 500 °C (H500). (c) EPR spectrum of Au/TiO_2 treated at 500 °C reveals a new signal at g = 1.930, assigned for Ti^{3+} defects. Reprinted with permission from.[56] Copyright American Association for the Advancement of Science, 2017. (d) In situ DRIFT spectra of CO adsorption deduced on Au/TiO_2 catalysts with different size of Au NPs and various facets of TiO_2 support. Reprinted with permission from.[61] Copyright Wiley-VCH GmbH, 2021.

samples. Among facets of TiO_2, samples with {101} facet showed no change of CO adsorption peak before and after the SMSI treatment, but samples with {100} and {001} did. TEM and HRTEM visualized SMSI encapsulation on the series of Au/TiO_2 samples. Full encapsulation took place with 5 nm Au NPs whereas for 2 nm Au NPs the partial encapsulation occurred instead. In brief, Au NPs with the size of 5 nm are likely to undergo SMSI than those of 2 nm and the SMSI are more favourable on {100} and {001} facets of TiO_2. DFT calculation explained that Au-TiO_2 SMSI promotes the reduction of TiO_2, especially at a greater extent on {100} and {001}. In addition, Zhang *et al.*[61] detected downward surface band bending of TiO_2 after SMSI treatment due to XPS binding energy shifts of Ti 2*p* and O 1s. The shift of Au 4*f*, Ti 2*p*, and O 1s supposed that charge transfer derives from surface oxygen vacancies of reduced TiO_x to Au NPs, not stoichiometric TiO_2 surface. Additionally, charge transfer at the Au-TiO_x interface is less extensive in the case of 2 nm Au NPs because of contracting lattice and depleted "*d*" orbitals, this impeding Au-TiO_2 SMSI.[61]

3. Approaches to generate strong metal-support interactions

Various techniques supply high energy to induce defects and valence variation of metallic species that are key factors for the migration of transition metal oxide support, leading to the so-called strong metal-support interaction.

3.1. High temperature annealing in a reductive environment to induce permeable/porous SMSI overlayers

One of the most common methods to generate SMSI encapsulation is high temperature annealing in a reductive atmosphere. Beck *et al.*[62] induced SMSI encapsulation of Pt on TiO_2 by annealing Pt/TiO_2 catalyst at 600 °C in H_2 or O_2. The encapsulation can be constructed through the migration of metal oxide support onto metal nanoparticles, and bimetallic alloy formation. This study also revealed the role of O_2 in the formation process and stabilization of the metal oxide overlayer. *In situ* transmission electron microscopy (TEM) was used to study the formation of SMSI over the time. After the samples were heated at 600 °C under 1 bar of H_2, platinum surface was gradually decorated and then fully covered within minutes. Once the samples were submitted to oxidative environment (under O_2 flow), an increase of the volume and crystallinity of metal oxide overlayer was observed. Electron energy loss spectra (EELS) of Ti under H_2 atmosphere showed a downward shift energy of 1 eV, reflecting partial titania reduction. TiO_2 overlayer covering Pt NPs was found to shrunk in size and Pt lattice at TiO_2-Pt interface showed a deformation. When O_2 oxidation atmosphere was replaced by H_2, structural defects appeared and the reconstruction of Pt NPs took place followed by a crystalline layer covering up of metal NPs. This layer involved multilayer of titania, which suggested a multistep support migration. *In situ* XPS provided insight on the surface-sensitivity of Pt/TiO_2 catalyst. Under H_2 atmosphere, Pt was found in fully reduced state, assigned with a peak of Pt $4f_{7/2}$ at 71.3 eV. The binding energy peak shifted of 0.8 eV to 72.1 eV when inlet gas was changed to O_2. The authors inferred the formation of Pt-O at the interface between Pt and TiO_2 overlayer, whereby electron transfer could take a place among the metal species and the metal oxide support. Near edge X-ray absorption fine structure (NEXAFS) – an extremely surface sensitive technique – confirmed the amorphous phase of TiO_2 overlayer under H_2 treatment while a typical spectrum of rutile was observed under O_2. The annealing method did not generate TiO_2 anatase, which is the most active phase and common-used in photocatalysis. Pt-Ti alloy formation, which is the second mechanism for SMSI encapsulation, was further clarified by *in situ* X-ray diffraction. A shift of Bragg peak of Pt into higher angles derived from lattice contraction which is attributed to the incorporation of Ti into Pt crystal structure. In other words, high temperature annealing under H_2 generated Pt-Ti bimetallic bonds as expectation.

Zhao *et al.*[63] used H_2 reduction treatment at high temperature to induce SMSI on TiO_2-supported Ir NPs. Strong metal-support interaction among Ir NPs and TiO_2 support was found effective on boosting the pairwise selectivity of propene hydrogeneration due to electronic and geometric blocking effects. Scanning transmission electron microscopy – high angle annular dark field (STEM-HAADF) images illustrated the discrepancy between two fresh catalyst specimens, which underwent calcination at 200 °C and 500 °C. Ir NPs observed larger size and flatter shape after reduction at 500 °C that could be a result of SMSI. In addition, any traces of TiO_2 amorphous layer were detected on the top of Ir NPs by STEM – annular bright field (STEM-ABF) imaging. ^{1}H NMR spectroscopy recorded reversible changes in the pairwise selectivity on a recycled catalyst specimen, which was re-oxidized in air at 400 °C and then reduced at 200 °C in H_2. Pairwise selectivity and overall catalytic activity remained unchanged after the recycling treatment. These findings further confirmed the presence of SMSI by means XPS analysis of the changes in oxidation states of metal species related to SMSI. Indeed, it would be challenging to determine the oxidation state of Ir because of the overlap between Ir 4*f* and Ti 3*s* peaks. Surprisingly, XPS spectra registered a broaden of Ti $2p_{3/2}$ peak (at 458.3 eV) in the case of Ir/TiO_2 annealed at 500 °C in H_2, ascribed to the reduction of Ti^{4+} to Ti^{3+}, which is a typical hallmark of SMSI formation.

Whilst previous studies identified high temperature treatment in a reductive environment as a key dimension of generating SMSI encapsulation, Liu et al.[64] has taken a reversed approach which constructed a permeable TiO_2 overlayer onto Au NPs under oxidative atmosphere, illustrated in Figure 4 (pathway a-d-e). Compared to the conventional pathway a-b-c, the reversed approach offered permeable SMSI overlayer without receding and re-oxidizing after being re-treated in air over 400 °C. The Au/TiO_2 catalyst was synthesized using deposition-precipitation method and then subjected to a modification step with melamine at 600 °C in N_2 followed by calcination at 800 °C in air. High-resolution transmission electron microscopy (HRTEM) depicted that the migration of TiO_2 encapsulated Au NPs after the calcination and melamine-induced encapsulation seems to withstand the sintering of Au NPs. In fact, the size of Au NPs observed an insignificant extension from 3.6 nm at the beginning to 7.5 nm after the final step. The metal nanoparticles without passing the melamine pre-treatment enlarged up to 32.6 nm in size because of an intensive sintering. However, the morphology and encapsulation of Au NPs with the size of less than 2 nm was not presented in this article.

This research assumed that high-temperature annealing with melamine in oxidative environment would encourage electron transfers from Au NPs to TiO_2 support, resulting in the reduction of Ti^{4+} to Ti^{3+} and positive charge on Au metal species, confirmed also by EELS and DRIFTS.[64] In addition, X-ray absorption fine structure techniques, including EXAFS and XANES, revealed almost fully occupied d orbital of Au and Au-Ti bond with a similar bond length to AuTi alloy. This finding could explain the migration of TiO_2 onto Au NPs. In other

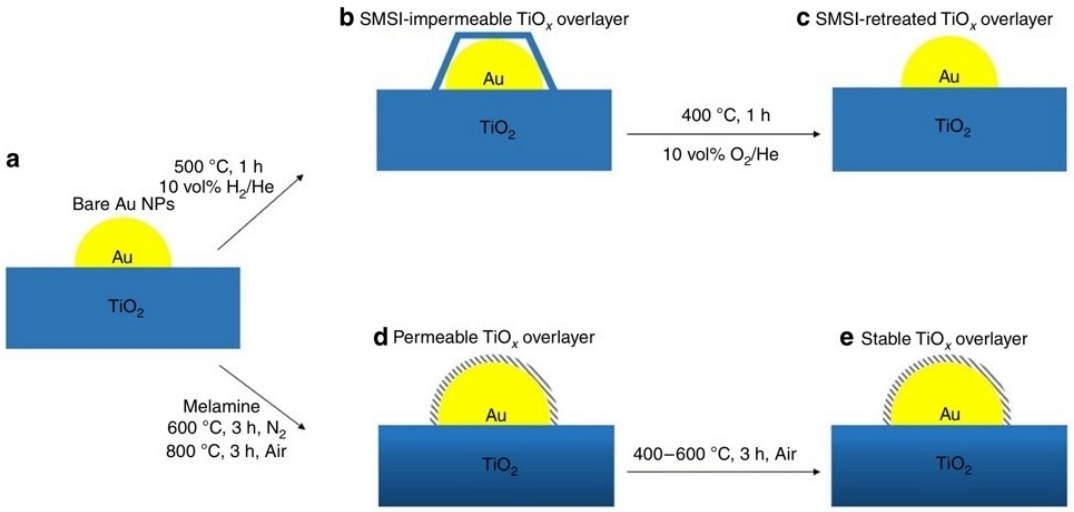

Figure 4. Two pathways to reach out TiO_x overlayer under high-temperature treatment: 1, Conventional SMSI encapsulation pathway starts from bare Au NPs deposited on TiO_2 support (a), followed by annealing at 500 °C in 10 vol% H_2/He to form an impermeable TiO_x overlayer (b). The SMSI-induced overlayer recedes as retreating at 400 °C under oxidative condition (c). 2, Melamine-induced SMSI encapsulation pathway involves annealing bare TiO_2-supported Au NPs (a) with melamine at 600 °C in N_2 to achieve a permeable TiO_x overlayer (d). This melamine-modified overlayer remains stable as retreating in air up to 600 °C (e). Reprinted with permission from.[64] Copyright Springer Nature, 2019.

words, SMSI encapsulation could be induced by a crystalline reconstructing of TiO_2 in the vicinity of Au NPs under an appropriate condition. TiO_2 overlayer was in anatase phase, which turns to rutile phase after calcination at 800 °C. While no trace of anatase phase was detected in the sample without undergoing melamine pre-treatment, the melamine-induced TiO_2 overlayer preserved 12% of anatase. Although the author reported SMSI between Au and TiO_2 is one of the key contributors to resist TiO_2 phase conversion, this approach suffers from the limited portion of the most active TiO_2 phase that hinders its availability in photocatalysis.

A great deal of previous research into SMSI has gone through high-temperature treatment. However, encapsulation processes under these conditions are generally uncontrollable and prompt, leading to limited exposure of active sites (Figure 5a). In fact, SMSI encapsulation layer are necessarily permeable to allow reactants to reach active sites, while the overlayer should fully encapsulate metal nanoparticles to preclude them from sintering and agglomeration, to cite a few, during catalytic reactions. To overcome these obstacles of the conventional SMSI, Wu *et al.*[65] proposed a porous yolk-shell structure of Pd-Fe_3O_4 which Pd atoms were expected to migrate into Fe_3O_4 crystalline structure (Figure 5b). During the procedure, Pd-FeO_x NPs were annealed at 300 °C under a mixture of H_2 and Ar atmospheres to trigger SMSI, in the meantime, another sample was treated at the same temperature but in air for comparison.

X-ray diffraction patterns indicated the amorphous phase of iron oxide shell as treating in air, while characteristic patterns of γ-Fe_3O_4 lattice appeared in the case of sample treated under H_2 reductive condition.[65,66] The g-Fe_3O_4 shell showed a microporous structure in HR-STEM images. The

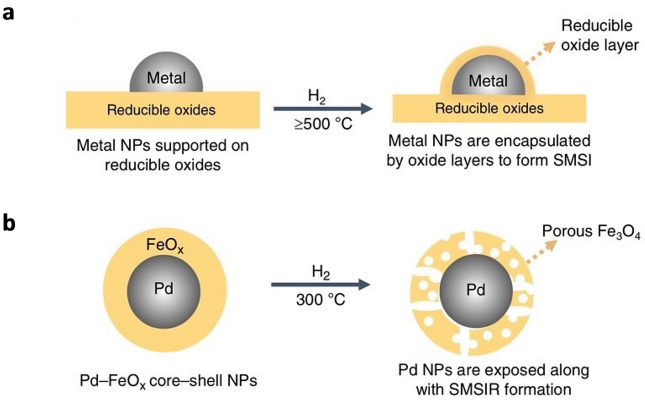

Figure 5. A reversed route to induce SMSI on Fe_3O_4@Pd core-shell nanostructure under H_2 reductive environment. The approach aims to compensate shortcomings of conventional SMSI. Reprinted with permission from.[65] Copyright Springer Nature, 2020.

research inferred that H_2 might reduce metal oxides at high temperature to generate oxygen vacancies in the oxide matrix. Meanwhile, the crystallization accompanies with redistribution of atoms in oxide grains that might accelerate the formation of oxygen vacancies, and thus a crystalline structure showing voids and cavities. Reactants are more likely to diffuse into pores and expose to metallic active sites, while the core-shell structure still guarantees SMSI such an electron transfer from Pd to Fe_3O_4.

A great number of groups have paid effort on SMSI of platinum-group metals, mainly Pt and Pd, under H_2 reductive condition. To escape from these boundaries, Li *et al.*[67] conducted research on Ni and anatase TiO_2 and pinpointed the role of NH_3 treatment together with H_2 treatment in SMSI formation. Ni species were deposited on two different

supports: 1)- anatase TiO_2 treated at 600 °C in NH_3 and 2)-anatase TiO_2 without experiencing the NH_3 treatment, both samples went through annealing in H_2 at 500 °C (Figure 6a). Surprisingly, the sample which Ni NPs were deposited on NH_3-treated anatase TiO_2 showed a superior catalytic activity and selectivity for CO_2 methanation, raising a question about the influence of NH_3 on the surface catalyst modification. XRD patterns showed no change in the anatase TiO_2 phase before and after NH_3 treatment. X-ray photoelectron spectroscopy showed the presence of nitrogen component as N 1s signal was recorded for anatase TiO_2. The N1s signal disappeared upon exposition to H_2 reduction, demonstrating that N-doping is unrelated to the enhancement of catalytic reaction yield. EPR studies showed an obvious signal at g-value of 1.987, which is typical of Ti^{3+} in bulk,[68,69] for NH_3-treated anatase TiO_2, whilst none was recorded for anatase TiO_2 (Figure 6b). Further investigation reported a proportional relation between the intensity of the Ti^{3+} EPR signal and CO_2 conversion yield (Figure 6c). HAADF-STEM, quasi – *in situ* XPS, and XRD provided some evidence of SMSI encapsulation. Ni NPs were efficiently dispersed over anatase TiO_2 without through NH_3 treatment, resulting in smaller crystal size of 9.5 nm (14.2 nm observed for Ni NPs on NH_3-treated anatase TiO_2). A larger size of Ni NPs and reduced Ti species (Ti^{3+}) in bulk might suppress the migration of TiO_2, leading partial encapsulation of Ni active sites. When skipping NH_3 treatment, Ti species remain in Ti^{4+} oxidation state, which were reduced by H_2 in the annealing step that would generate full encapsulation of Ni. In this study, the authors considered that TiO_2 overlayer could inhibit the exposure of reactants to Ni active sites, and thus deteriorate catalytic activities.

3.2. The SMSI construction mediated by adsorbates

Matsubu *et al.*[70] reported the customization of SMSI on TiO_2-supported Rh catalyst to tune selectivity of CO_2 reduction reaction through use of treatment in a CO_2-H_2 mixed environment at 150–300 °C. The catalytic CO_2 reduction on Rh/TiO_2 catalyst (Figure 7a), which experienced a treatment in CO_2:H_2:He (20:2:78 v/v ratio) at 250 °C, registered a decrease in CH_4 production rate but an increase in CO production rate. At the beginning, the disintegration of Rh NPs into isolated Rh atoms was supposed. However, *ex situ* scanning electron microscopy does not show any change in Rh structure. *In situ* diffuse reflectance infrared Fourier transform spectroscopy (DRIFTS) revealed a high coverage of HCO_x adsorbates, including formate and bicarbonate-like species, on TiO_2 surface during the $20CO_2$:$2H_2$ treatment. At temperature higher than 100 °C, the adsorbate coverage could generate oxygen vacancies on TiO_2 surface, resulting in a migration of TiO_2 onto Rh active sites. *In situ* STEM and *in situ* EELS showed that the TiO_2 overlayer exists in amorphous phase, involving Ti^{3+} (30%) and Ti^{4+} (70%). In contrary to a conventional SMSI overlayer exclusively induced in H_2 at 500 °C, HCO_x-induced SMSI overlayer was permeable, porous, and partially reduced. In addition, HCO_x adsorbates coordinated with Ti species and stabilized SMSI encapsulation during catalytic reactions.

The reduction of metal oxide support has been identified as a prerequisite for SMSI encapsulation. However, critical conditions, involving high temperature at 100 °C in either generally inert or reductive atmosphere, became main obstacles for experimental approaches of inducing SMSI. Some research reported that alcohol could foster the reduction of metal oxides,[72,73] especially below 100 °C in the case of TiO_2.[74] In order to address the aforementioned issues, Polo-Garzon *et al.*[71] studied alcohol-induced SMSI at low temperature. TiO_2-supported Au catalyst was treated in *iso*-propanol or methanol at 30 °C prior to another treatment in argon at

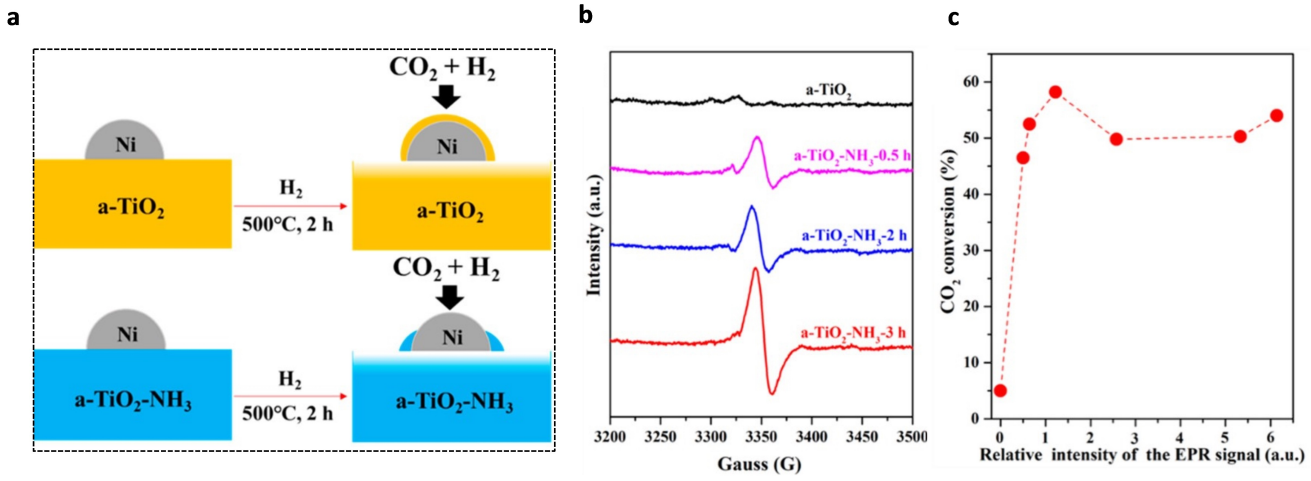

Figure 6. (a) Schematic illustration of inducting SMSI in high-temperature H_2 atmosphere on anatase TiO_2 support with and without undergoing ammonia treatment. (b) EPR spectra recorded at 110 K for anatase TiO_2 and anatase TiO_2 after being annealing in NH_3 atmosphere within different durations. (c) The correlation between EPR signal intensity and CO_2 conversion yield. Reprinted with permission from.[67] Copyright American Chemical Society, 2019.

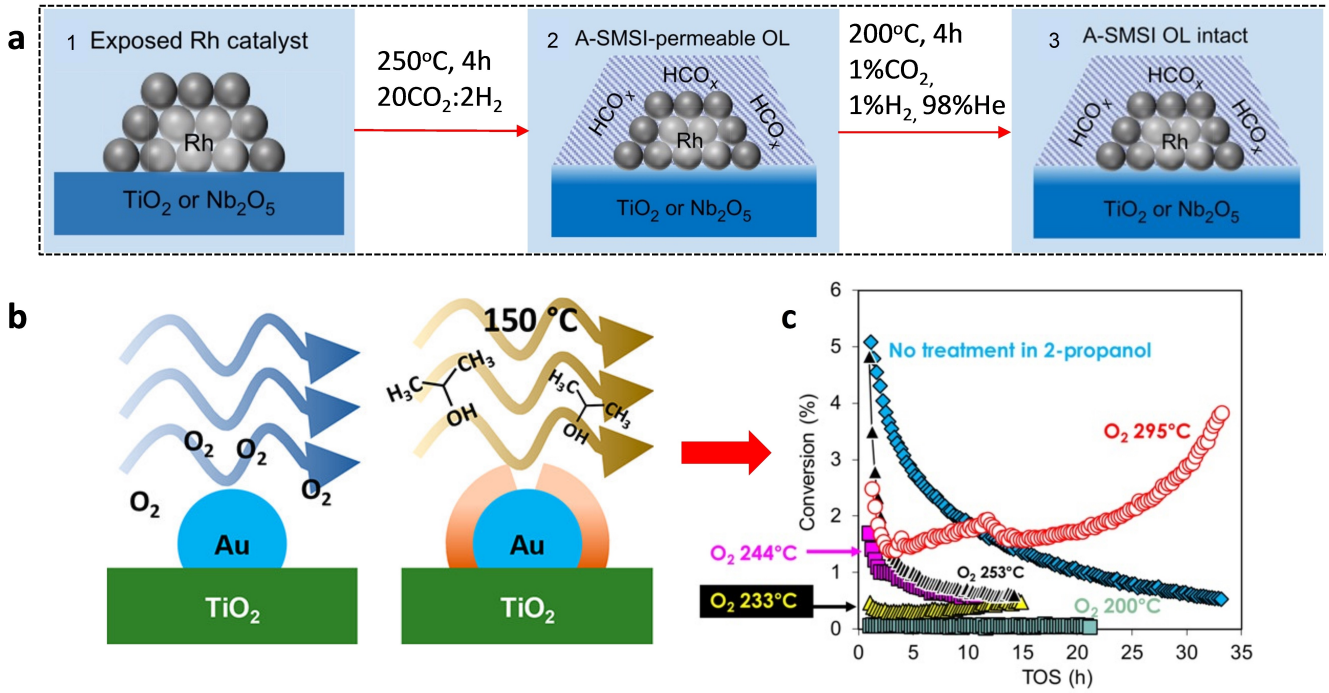

Figure 7. (a) Schematic illustration of adsorbate-induced SMSI formation: 1, bare TiO_2-supported Rh nanoparticles favours to reduce CO_2 to CH_4. 2, Treatment in CO_2 and H_2 produces a permeable overlayer consisting of TiO_x species and HCO_x adsorbates. 3, The SMSI overlayer remains intact during and after catalytic CO_2 reduction reactions. Reprinted with permission from.[70] Copyright Springer Nature, 2016. (b) 95% of Au active site encapsulated by TiO_2 support after a treatment in iso-propanol at room temperature followed by desorption at 150 °C. (c) The time-on-stream (TOS) rate of CO conversion after treating in O_2 at different temperature to retract TiO_2 overlayer, divulging the so-called "self-activating" (right). Reprinted with permission from.[71] Copyright American Chemical Society, 2020.

300 °C to flush adsorbed alcohol molecules. A decrease of infrared spectroscopic (IR) peaks of CO adsorption evidenced the inaccessibility of Au active sites. The authors further studied to elucidate at which process, either exposure to 2-propanol at 30 °C or desorption of 2-propanol by Ar flushing at elevated temperature. They found metal sites were only partially covered during the first step. A full coverage was really reached upon 150 °C when the desorption/decomposition of alcohols might trigger chemical transformation of catalyst surface. The alcohol-modified catalyst then experienced the final treatment in O_2 at around 250 °C (Figure 7b). The authors recorded partial receding of the TiO_x overlayer on Au species, unfolding a larger number of catalytic sites and thus curtailing catalytic deactivation, which was characterized by the increasing red curve in time-on-stream rate (TOS, Figure 7c).

3.3. Laser treatment and photoinduced SMSI encapsulation

So far, universal methods of constructing SMSI encapsulation in various environment under ambient conditions are still in high demand. Laser ablation has known as a universal, green, and practical method in synthesizing metal-mediated nanomaterials. However, nanosecond and longer pulse irradiation generally suffer from high temperature and high pressure that might initiate unfavourable phase transformation and/or sintering of metal active sites. Thus, ultrafast pulse laser, involving femtosecond and picosecond, could address the drawbacks based on its ultrahigh intensity but ultrashort irradiation time. Taking these advantages of femtosecond laser excitation (35 fs), Zhang *et al.* succeeded in inducing SMSI on CeO_2-supported Pt NPs, evidenced by porous/permeable overlayer of CeO_2 onto Pt NPs.[75] When triggering the pulse laser at the interface, local plasmon resonance of Pt contributes to electric field enhancement, resulting in ionization of CeO_2. In particular, the flux of photons is likely to excite electrons to conduction band and leave holes at valence band. Surface oxygen atoms would donate electrons to compensate the electronic imbalance, leading to a high probability to be peeled off. The mechanism was shown in Figure 8a. As a result, surface defects, including Ce^{3+} and oxygen vacancies were detected by EPR and XPS. Such CeO_x species tend to reorganize its structure and then migrate to encapsulate partially Pt NPs. This study showed that the thickness of the metal oxide overlayer was proportional to laser exposition time.[44] The author recorded none of these phenomena on laser-treated pure CeO_2. This emphasized the role of the enhanced electric field at metal – metal oxide interface in the formation of surface defects. The study reported SMSI encapsulation of metal NPs not only on reducible metal oxide such as Pt/TiO_2, Pd/TiO_2, and Au/TiO_2, but also non-reducible metal oxides, including Pt/Al_2O_3, Pt/SiO_2, and Au/MgO.

Another photochemistry-driven methodology was reported for the construction of SMSI on TiO_2-supported Pd catalyst under ambient conditions.[14] The SMSI generation

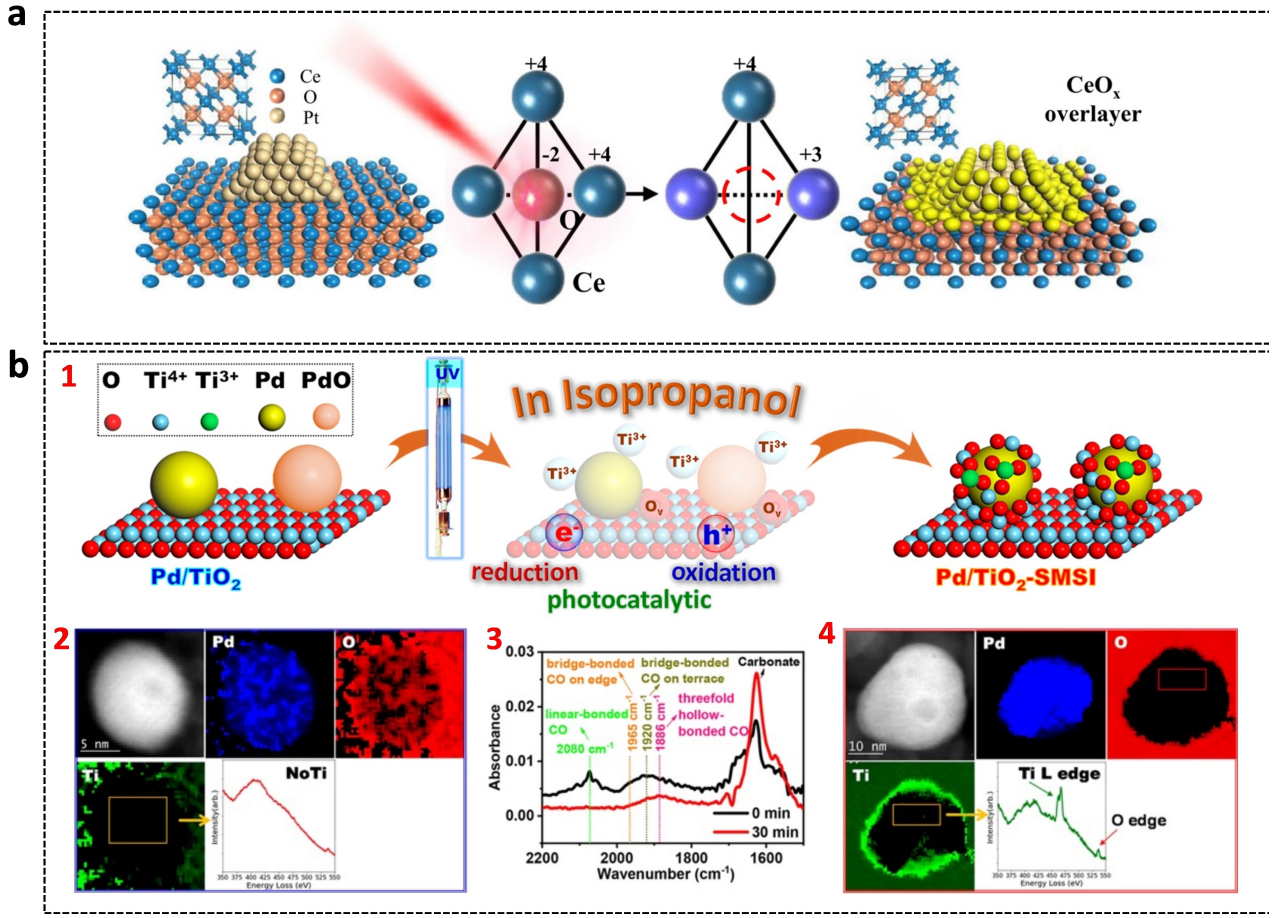

Figure 8. (a) Ultrafast laser induces oxygen vacancies and Ce^{3+}, leading to SMSI encapsulation of Pt NPs by CeO_x overlayer. Reprinted with permission from.[75] Copyright Springer Nature, 2021. (b) 1. Two-step pathway to achieve SMSI encapsulation of Pd NPs supported over TiO_2 in isopropanol under UV irradiation 2. STEM-ADF images and EELS spectrum at Pd site show no coverage of TiO_2 3. Suppressed CO adsorption on Pd sites after 30 minutes of UV illumination 4. STEM-ADF images and EELS spectrum at Pd site after UV treatment demonstrates TiO_2 overlayer onto these metal sites. Reprinted with permission from.[14] Copyright American Chemical Society, 2021.

leans on the formation of Ti^{3+} and oxygen vacancies which were triggered by photo-excited charge carriers (reductive electrons and oxidative holes). Instead of using ultrafast laser, a dispersed solution of Pd/TiO_2 in isopropanol was irradiated by a UV lamp at room temperature (Figure 8b.1). Photo-generated electrons in TiO_2 bulk could diffuse to surface and reduce Ti^{4+} to Ti^{3+} species, which are then dissolved in the solution. The Ti^{3+} species accumulate on Pd NPs due to Ti^{3+} -metal interaction, resulting in Pd-O_{vacant}-Ti^{3+} sites at the interface. These interfacial sites seem to be the prerequisite for SMSI encapsulation. The STEM-ADF images and EELS mapping evidenced the formation of TiO_2 overlayer onto Pd species (Figure 8b.2 and Figure 8b.4). Through XRD patterns, the author recorded the anatase phase of the overlayer and metallic phase of Pd (111), while the characteristic peak of Pd (111) showed a downward trend over UV irradiation time. Surface-induced amorphization, decreased crystalline size, and lattice expansion of Pd NPs under a long UV-irradiation time. The suppression of CO adsorption, investigated by CO-DRIFTS, once again confirmed the SMSI encapsulation of Pd NPs. Particularly characteristic peaks of linear CO adsorption and bridged CO adsorption on edge and terrace of Pd^0 (green, orange, and greenish beige) were observed in CO-DRIFTS spectrum of Pd/TiO_2 after 30 minutes of irradiation (Figure 8b.3), while the peak of threefold-hollow-bonded CO remained insignificant (pink).

3.4. Wet chemistry to construct SMSI encapsulation

In general, conventional method to create SMSI overlayer involves the migration of reducible metal oxide support onto metal nanoparticle active sites through redox treatments at high temperature. However, those metal NPs are likely to undergo agglomeration and sinter into bigger clusters. In addition, a receding of the metal oxide overlayer could operates during the catalytic reaction. Zhang *et al.* proposed a "wet-chemistry" SMSI (wcSMSI) to produce TiO_x overlayer onto Au NPs but at room temperature.[55] TiO_2-supported Au catalyst was firstly synthesized by deposition-precipitation method

(Figure 9a). Then, a TiO_x colloid solution, prepared from the gradual hydrolysis of $TiCl_3$ in a basic media $NaHCO_3$, was dropped into the Au/TiO_2 in liquid phase. In this case, Au NPs typically play a role of nucleation seeds for TiO_x encapsulation. This study reported the mean diameter of Au NPs at 2 nm, which is smaller than that reported in previous articles.[56,76] *Operando* FTIR unveiled partial coverage of Au NPs by TiO_x overlayer and electronic interaction between Au NPs and TiO_x, evidenced by weaker band of CO adsorption and their shift under different treatments. In fact, the authors identified Au-Ti^{3+} interaction as the key for the wcSMSI generation, which was highlighted by XPS. Looking at Au 4*f* region in XPS spectra (Figure 9b) pre-treated Au NPs in O_2 showed two peaks at 83.8 eV and 84.7 eV assigned to metallic Au^0 and oxidized $Au^{\delta+}$ species. These peaks became negligible when adding Ti^{3+} into Au colloid, while characteristic peaks of reduced $Au^{\delta-}$ species became predominant.

Meantime, Ti 2*p* region in XPS spectra (Figure 9c) exhibited the disappearance of Ti^{3+} peaks at 457.1 eV. This could be explained by the reduction of Au species by Ti^{3+}.

Another research from our group introduced a facile procedure to obtain SMSI via soft chemistry.[77,78] The key idea lies in depositing substoichiometric TiO_x onto Au NPs which are both supported on SiO_2 microspheres, constructing core@-shell nanostructure (Figure 9d). Compared to amorphous and non-stoichiometric TiO_x overlayer induced by classical method under reductive and high temperature conditions, the soft-chemistry approach offered SMSI-like TiO_x layer in photoactive anatase phase with adjustable thickness (Figure 9e). Combining with local surface plasmonic resonance of Au NPs, the authors firstly reported the use of soft-chemistry SMSI concept in photocatalysis. Under UV-visible illumination, photogenerated electrons were excited to jump to conduction band of TiO_2. These electrons transferred from TiO_2 conduction band to Au NPs, which act as electron reservoirs due to metal – semiconductor Schottky junction. Surprisingly, the electrons were injected back from Au NPs to TiO_2 even accompanied with the injection of gold LSPR "hot" electrons, evidenced by time-resolved microwave conductivity analysis. In addition, the catalysts prepared by soft-chemistry method were also active in thermal catalysis. The SiO_2@Au@TiO_2 was studied in base-free furfural oxidation at relatively low temperature (110 °C). The enhanced catalytic behaviour of these materials compared to classical supported Au catalysts suggests an essential role of the TiO_2 overlayer on Au nanoparticles. Encapsulation prevents Au not only from leaching but also from Au deactivation by irreversible furfural adsorption.[79] This soft-chemistry left a perspective on developing SMSI encapsulation on other metals such as Pt, Cu, and Ni.

3.5. Mechanochemistry-driven SMSI encapsulation

Solid-state approaches to chemical synthesis and materials science have gained more and more attention in last years. Mechanochemistry became potential to carry out solid-state reactions because it is clean, safe, and facile.[80] In fact, simple methods, which are able to induce controllable SMSI, specifically under ambient conditions, and tailor encapsulation extent as well as SMSI structures, are in high demand. As a result, several research groups developed mechanochemistry-driven approaches to construct SMSI. Zhang *et al.*[81] reported

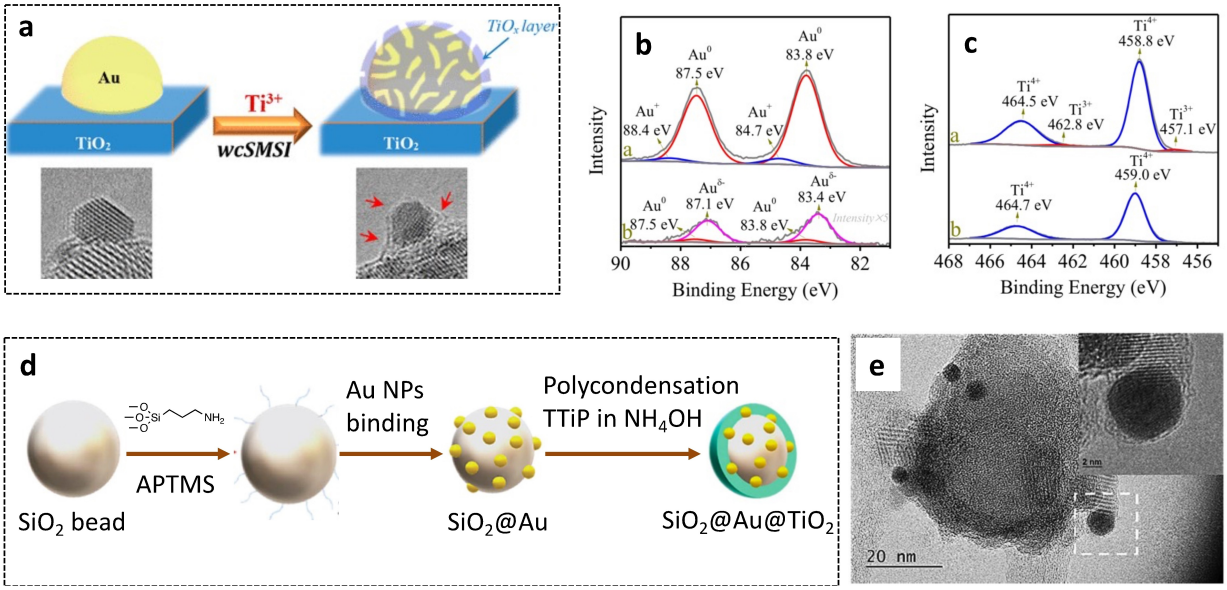

Figure 9. (a) Wet-chemistry SMSI encapsulation of Au NPs through Ti^{3+}-Au interaction in liquid phase. (b) Au 4f XPS spectra of Au NPs when pre-treated in O_2 (above) and adding Ti^{3+} (below). (c) Ti 2p XPS spectra of TiO_x colloid before (above) and after (below) interacting with Au NPs. Reprinted with permission from.[55] Copyright American Chemical Society, 2019. (d) Schematic illustration of constructing SMSI-like TiO_x overlayer on Au NPs via a soft-chemistry pathway. (e) HRTEM image of an encapsulated Au NPs. Reprinted with permission from.[77] Copyright Royal Society of Chemistry, 2020.

SMSI encapsulation on TiO_2-supported Pd and TiC-supported Pd electrocatalysts through the use of mechanical milling under ambient atmosphere (Figure 10a). HRTEM illustrated TiO_x overlayers on Pd/TiO_2 in which their thickness could be adjusted by milling time, while XRD determined amorphous phase of these overlayer. In addition, SMSI imposed some modification on electronic structure of Pd NPs. Particularly, the decreasing intensity of Pd^{2+} peaks and the increasing of $Pd^{\delta-}$ peaks in XPS spectra over milling time was observed (Figure 10b). A similar pattern was seen on Ti 2*p* with a dominant intensity of low valence state and a fading intensity of high valence state (Figure 10c). These experimental outputs demonstrate a reduction of both Ti and Pd. In other words, SMSI might accelerate a reduction of TiO_2 and hence a reduction of Pd due to charge transfer.

Recently, Ti^{3+} and oxygen vacancies, which are the key of SMSI encapsulation, were generated on Pd/anatase TiO_2 catalyst using a $NaBH_4$-assissted mechanochemical method under ambient conditions (Figure 10d).[82] Strong reducing agent such as $NaBH_4$ can reduce Pd^{2+} and Ti^{4+} to Pd^0 and Ti^{3+}, respectively, as evidenced by XPS. SMSI encapsulation of Pd NPs by TiO_x overlayer leaded to lower chemisorbed CO amount. The CO adsorption showed a downward trend upon increasing ball milling time, reflecting its capability of regulating encapsulation extent. High-speed vibrant ball milling encourages energetic solid-state interactions, resulting in rapid transfer of these reactive intermediates. Indeed, Ti^{3+} could adsorbed on Pd NPs during high-interactive conditions. Combining with oxygen vacancies, Pd-O_v-Ti^{3+} sites could be generated and thus SMSI encapsulation (fig. 10e). This study demonstrated the mechanochemistry-driven pathway could initiate SMSI on different metal NPs (Pd, Ru, and Pt) supported on a variety of reducible metal oxides, including TiO_2, ZnO, Fe_3O_4, and Nb_2O_5.

4. Strong metal-support interaction in photocatalysis

So far, strong metal-support interaction has been largely neglected in photocatalytic reaction, and only few studies have been reported. Lin *et al.*[33] constructed SMSI between Pt nanoparticles homogenously dispersed on oxygen-vacancy defective TiO_2 crystalline for gas-phase photocatalytic CO_2 reduction. Pt NPs were partially covered by disordered TiO_2 layers through a high-temperature flame aerosol synthesis. While CO_2 photoreduction on bare TiO_2 produced CO only, CH_4 was detected additionally from the photoreduction reactions on Pt-modified TiO_2. Indeed, SMSI between Pt and TiO_2 obviously tuned the selectivity of CO_2 photoreduction thanks to electron transfer from TiO_2 to Pt NPs. The authors reported that Pt-supported oxygen-vacancy induced TiO_2 photocatalyst resisted catalytic deactivation after eight-hour

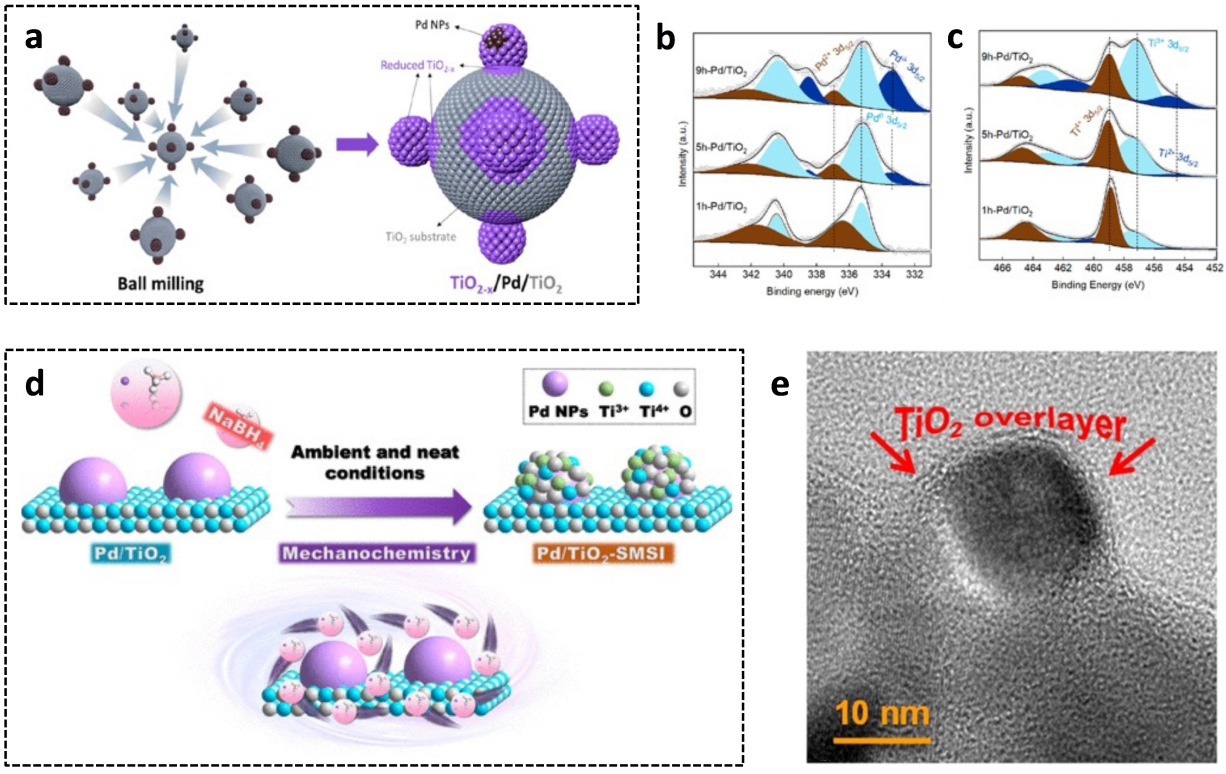

Figure 10. (a) Encapsulation of TiO_x overlayer onto Pd NPs supported on TiO_2 P25 or TiC through mechanochemical ball milling. (b) Pd 3d XPS spectra and (c) Ti 2p XPS spectra of Pd/TiO_2 over prolonging milling time. Reprinted with permission from.[81] Copyright American Chemical Society, 2022. (d) Mechanochemical $NaBH_4$-driven SMSI encapsulation of Pd NPs on anatase TiO_2. (e) HRTEM images of the SMSI TiO_x overlayer. Reprinted with permission from.[82] Copyright American Chemical Society, 2022.

photoreaction because of SMSI on ruling out Pt and oxygen vacancies. In this case, oxygen vacancies tend to strengthen CO_2 adsorption on photocatalyst surface, thus boosting photocatalytic efficiency. The selectivity toward methane was explained by studying different pathways of CO_2 adsorption and activation during photocatalytic reduction in the presence of H_2O (Figure 11a). In details, adsorbed CO_2 would react with OH groups on the surface of bare O_v-defected TiO_2 to form CO_3^{2-} intermediates, which can be further converted to CO and CH_4. In the case of Pt-mediated photocatalysts, Pt NPs become active sites for heterolytic dissociation of H_2O to H^+ protons. Besides, electron transfers from TiO_2 to Pt resulted from SMSI made these metal NPs act as electron reservoirs. CO_2 molecules in the vicinity of SMSI regions would capture those electrons and together with H^+ protons to produce

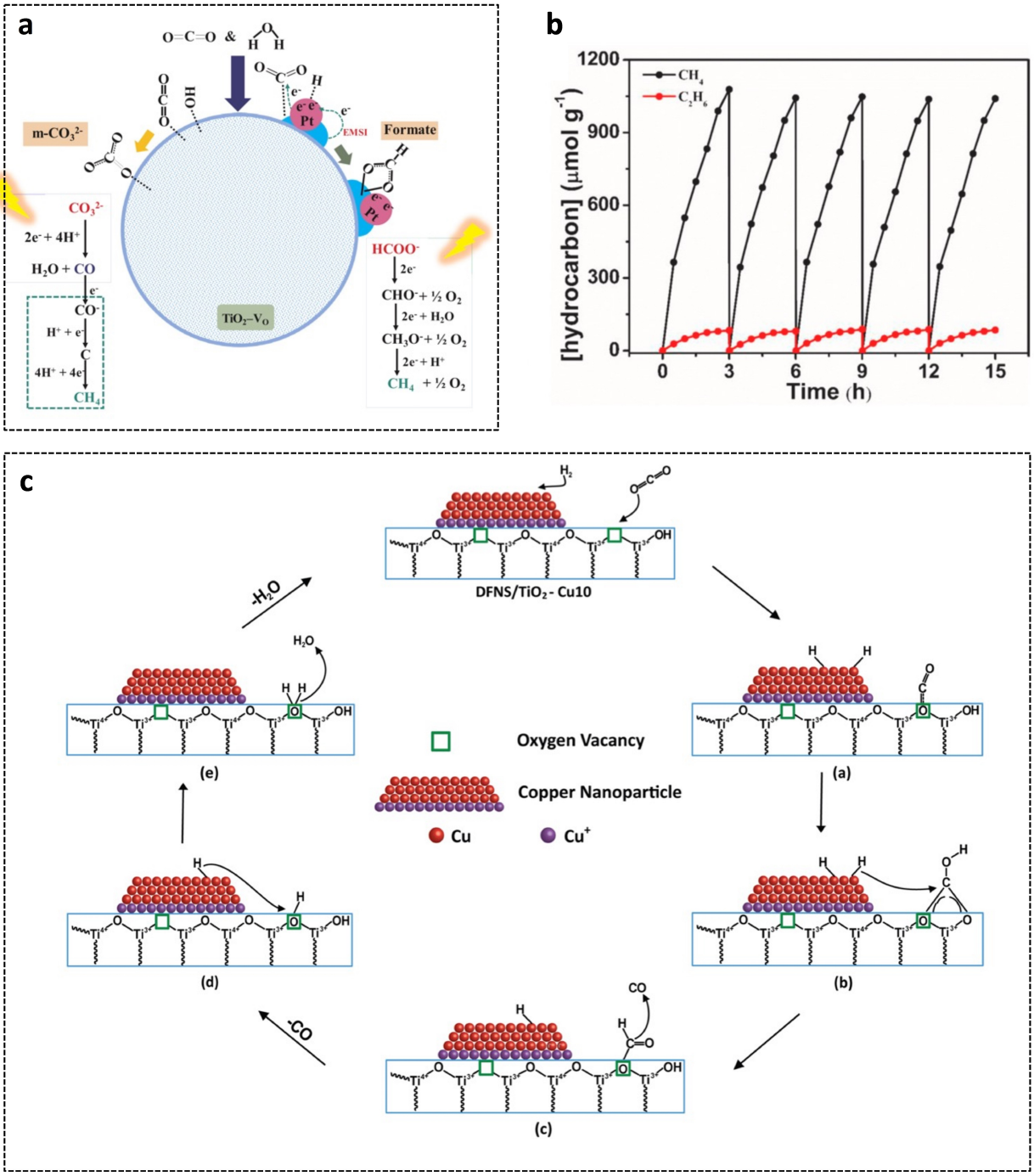

Figure 11. (a) Different pathways of CO_2 photoreduction with H_2O on bare TiO_2 and defective TiO_2-supported Pt photocatalysts. Reprinted with permission from.[33] Copyright Elsevier, 2020. (b) Hydrocarbons, CH_4 and C_2H_6, production on single-atom binary metal components supported on TiO_2 nanotubes from CO_2 photoreduction. Reprinted with permission from.[83] Copyright Elsevier, 2021. (c) A proposed mechanism for CO_2 reduction to CO on TiO_2-coated dendritic fibrous nano-silica supported Cu catalysts. Reprinted with permission from.[84] Copyright American Chemical Society, 2023.

formate species ($HCOO^-$), which is further reduced to CH_4 (Figure 11a)

Another research on enhancing gas-phase photocatalytic CO_2 reduction in water vapour phase was reported on strong metal-support interaction between single-atom binary metal components Pt/Au and TiO_{2-x} nanotube.[83] These metal components were supposed to trap electrons and create bonds with uncoordinated Ti^{3+} sites, inducing electron transfers from Ti^{3+} to Pt and Au. This study assigned the conversion of CO_2 into $CO_2^{\bullet-}$ as a rate-limiting step of the photocatalytic reduction. Electron-rich bimetal components might boost multi-electron reactions, evidenced by the modification of one-electron water oxidation to four-electrons, leading to O_2 evolution instead of $^{\bullet}OH$ generation. Catalysts mediated with atomic scale Pt and Au clearly promoted the polarization of CO_2 and protonation of $CO_2^{\bullet-}$ to $^{\bullet}CH_3$ radicals, resulting in CH_4 or C–C coupling to C_2H_6. The catalytic activity remained stable after five testing cycles (Figure 11b).A recent study has reported strong metal-supported interaction on TiO_2-supported Cu catalyst and its use in CO_2 reduction reaction.[84] TiO_2 support partially encapsulated and induced SMSI overlayer around Cu active sites where Ti^{3+} species found them strongly bond with copper atoms, accompanying with defective oxygen vacancies on TiO_2 surface. This study proposed a mechanism of CO_2 reduction, illustrated in Figure 11c. CO_2 molecules adsorbed on TiO_2 surface through filling oxygen vacancy defects before reacting with hydroxyl group to produce bicarbonate species and then formate intermediates by dissociated H from Cu NPs. The formate intermediates would break down into CO and leave OH on TiO_2 surface which desorbed as water molecules after reacting with another dissociated H species. Afterwards, the catalyst regenerated oxygen vacancies and Ti^{3+} species as a fresh one.[84]

Strong metal-support interaction between Au NPs and TiO_x was firstly reported in the context of photocatalytic hydrogen evolution in a research by Gesesse *et al.*[77] In this study, the authors deliberately covered stoichiometric TiO_2 anatase overlayer onto plasmonic Au NPs dispersed on SiO_2 microspheres. The SMSI-like core@shell nanostructure recorded 10 times higher photocatalytic H_2 production yield than a conventional photocatalyst in which Au NPs were deposited on TiO_2 surface (Figure 12a). This could be attributed to hot electron injection from Au NPs to TiO_2 conduction band and superior charge carrier dynamics within the nanostructure. Time-resolved microwave conductivity (TRMC, Figure 12b) evidenced that Au NPs enable to prolong photogenerated charge carrier lifetime in which electrons could be not only transferred from TiO_2 to Au NPs, but also injected back from Au NPs to TiO_2 through SMSI region, leading to superior charge carrier separation and boost photocatalytic efficiency. Density functional theory (DFT) calculation was performed to understand adsorption/desorption energy in the photocatalyst designs (Figure 12c). The stronger adsorption/desorption energy of methanol on TiO_2 surface (−1.0788 eV) in the case of conventional design explained its lower photocatalytic activity because of restraining desorption of methanol from the surface which is a crucial step in methanol aqueous solution of H_2 production. In order to achieve an optimal reaction yield, the adsorption sites of hydrogen ions should most likely occur at the Au/TiO_2 interface. In fact, the active sites cover a larger surface in the encapsulation design compared to the conventional design. In the case of conventional design, Au NPs are the active site. The distance between adsorption site and Au NPs is longer, leading to the limited probability of photocatalytic reactions.

5. Conclusions and Perspectives

In this manuscript, we reviewed the classical SMSI between platinum-group metals and reducible metal oxide such as TiO_2. It was believed that the SMSI encapsulation is exclusively able to occur onto the platinum-group metals which have high work function (> 5.3 eV) and great surface energy (> 2 $J.m^{-[2]}$) .[85] However, recent studies have already demonstrated that SMSI occurred with Cu (4.46 eV)[86] and Au (5.3 eV)[87] even on different metal oxide supports (TiO_2, ZnO, Nb_2O_5, CeO_2 etc.), leading to potential extension of SMSI concept in solid-state chemistry and material science. This review summarized a variety of synthetic approaches to induce SMSI, including high-temperature annealing, alcohol adsorbate-induced encapsulation, laser/photon irradiation treatment, wet chemistry, and the most recent mechanochemical technique. High temperature annealing in reductive environment is the most commonly used method. Because of impermeable TiO_2 overlayer after the treatment which could insulate metallic active sites and deactivate catalytic activity, some efforts have been devoted to generate a permeable overlayer through modifying synthesis procedure with melamine or architecting a porous structure of metal oxide support. The high temperature synthetic condition would be an obstacle that incentivized later attempt on alternative approaches at milder or ambient conditions such as isopropanol-adsorbate treatment and ultrafast laser inducing. Even though of successfully generating TiO_x overlayer onto metal NPs, these techniques generally failed to obtain high crystalline TiO_2 in anatase phase, but amorphous TiO_2. This typically limited the application of SMSI in the context of heterogeneous photocatalysis. In addition, it is necessary to call for methods that SMSI overlayer thickness is adjustable in purpose. Wet chemistry and mechanochemistry methods nominated themselves as potential choices to overcome these challenges. Strong metal-support interaction typically accompanies with fully or partially encapsulation of metal nanoparticles by metal oxide support. Electronic interactions through bonding between Ti element of TiO_2 and supported metal species induce electron transfer from TiO_2 to metal NPs, leading to Ti^{3+} species and oxygen vacancies O_v in SMSI region. These surface defects importantly play as active sites during (photo)catalytic reactions. In addition to electronic interaction, SMSI encapsulation exerts some effects on morphology of supported metal nanoparticles. The overlayer would exclude sintering, agglomeration and leaching of metal NPs or even metal nanoparticle lost during synthesis and catalytic reactions.

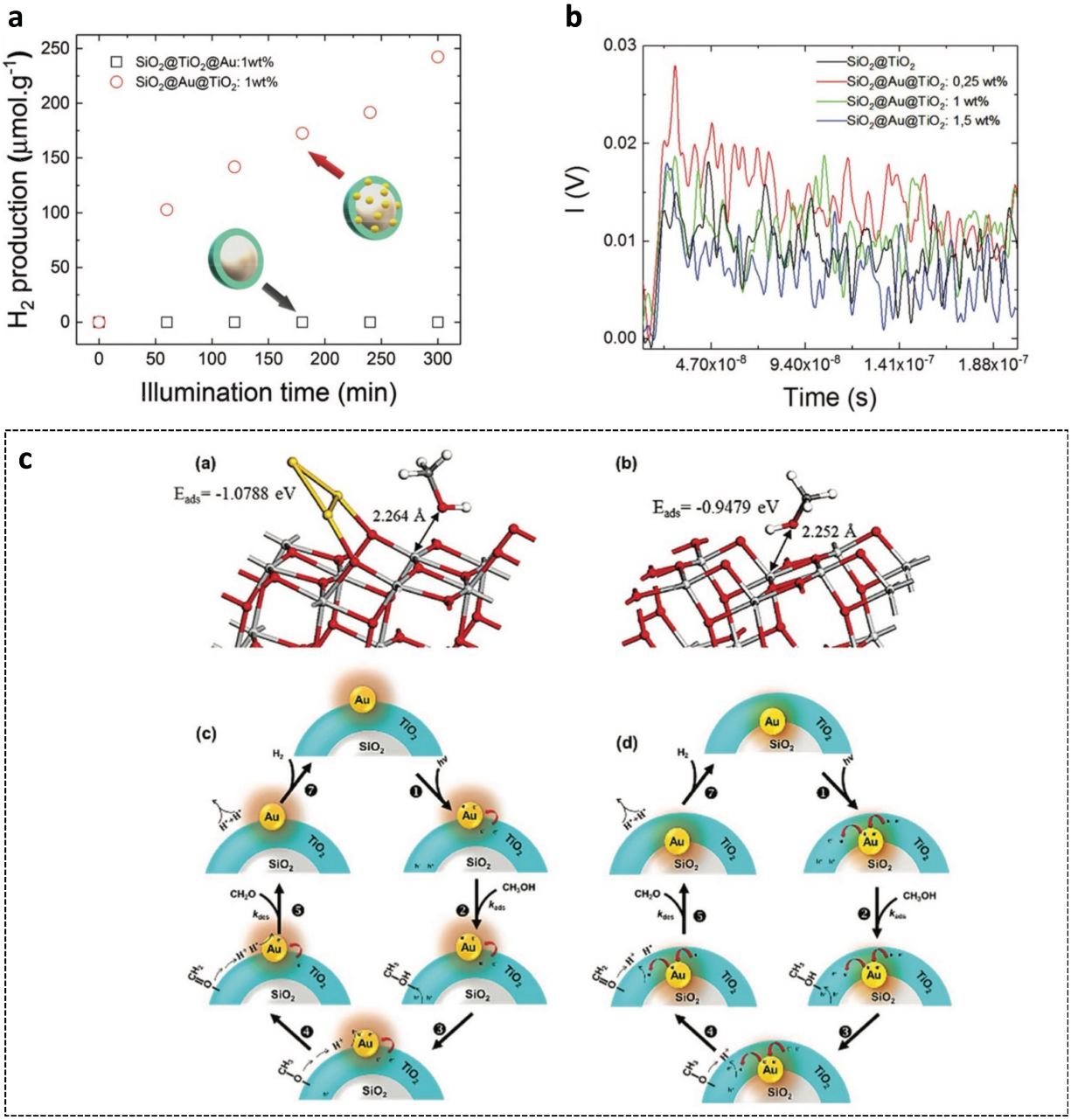

Figure 12. (a) Hydrogen production yield on SMSI-like core@shell SiO_2@Au@TiO_2 and conventional core@shell SiO_2@TiO_2@Au photocatalysts in methanol/water solution. (b) high intensity and long decay of time-resolved microwave conductivity signal reveal superior charge carrier dynamics within the SMSI-like nanostructure. (c) A proposed mechanism by DFT of methanol dissociation, reduction of H^+ species on the two different core@shell nanostructures. Reprinted with permission from.[77] Copyright Royal Society of Chemistry, 2020.

In conclusion, strong metal-support interaction has become promising to tune electronic properties and surface chemistry of metal nanoparticles highly dispersed on metal oxide support. There are still high demands of universal approaches to trigger SMSI at ambient conditions. Besides, a limited number of studies mentioning SMSI in photocatalysis leave a huge space for perspectives of architecting different SMSI-liked nanostructures, replacing noble metals (Pt, Pd, Au, etc.) by earth-abundant metals (Cu, Co, Ni, Fe, etc.) which could demonstrate improved photocatalytic activity, elevated stability, and reproducibility.

Acknowledgements

The authors thank the public grant overseen by the French National Research Agency (ANR) through the INGENCAT project (ANR-20-CE43-0014)

Conflict of Interests

The authors declare that they have no conflict of interest.

Keywords: strong metal-support interaction · SMSI encapsulation · TiO_2 · photocatalysis

[1] C. Wang, M. N. Ghazzal, *Energy Adv.* **2023**, *2 (7)*, 965–979.
[2] J. Li, X. Han, D. Wang, L. Zhu, M. Ha-Thi, T. Pino, J. Arbiol, L. Wu, M. Nawfal Ghazzal, *Angew. Chem.* **2022**, *134 (43)*, e2022102.
[3] Q. Xu, M. Knezevic, A. Laachachi, S. Franger, C. Colbeau-Justin, M. N. Ghazzal, *ChemCatChem* **2022**. *14 (12)*, e2022001.
[4] C. Wang, E. Paineau, H. Remita, M. N. Ghazzal, *Chem. Mater.* **2021**, *33 (17)*, 6925–6933.
[5] C. Wang, J. Li, E. Paineau, A. Laachachi, C. Colbeau-Justin, H. Remita, M. N. Ghazzal, *J. Mater. Chem. A* **2020**, *8 (21)*, 10779–10786.
[6] G. D. Gesesse, C. Li, E. Paineau, Y. Habibi, H. Remita, C. Colbeau-Justin, M. N. Ghazzal, *Chem. Mater.* **2019**, *31 (13)*, 4851–4863.
[7] D. A. Torelli, S. A. Francis, J. C. Crompton, A. Javier, J. R. Thompson, B. S. Brunschwig, M. P. Soriaga, N. S. Lewis, *ACS Catal.* **2016**, *6*, 2100.
[8] X. C. Sun, K. Yuan, J. H. Zhou, C. Y. Yuan, H.-C. Liu, Y. W. Zhang, *ACS Catal.* **2022**, *12 (2)*, 923–934.
[9] N. Sun, Y. Zhu, M. Li, J. Zhang, J. Qin, Y. Li, C. Wang, *Appl. Catal. B* **2021**, *298 (3)*, 120565.
[10] S. Hu, P. Qiao, X. Yi, Y. Lei, H. Hu, J. Ye, D. Wang, *Angew. Chem.* **2023**, *135 (26)*, e2023045.
[11] J. Li, Y. Lin, X. Pan, D. Miao, D. Ding, Y. Cui, J. Dong, X. Bao, *ACS Catal.* **2019**, *9 (7)*, 6342–6348.
[12] J. Liu, C. Li, F. Wang, S. He, H. Chen, Y. Zhao, M. Wei, D. G. Evans, X. Duan, *Catal. Sci. Technol.* **2013**, *3*, 2627.
[13] X. Yang, F. Tan, D. Wang, Q. Feng, D. Qiu, D. Dang, X. Wang, *Ceram. Int.* **2021**, *47 (19)*, 27316–27323.
[14] H. Chen, Z. Yang, X. Wang, F. Polo-Garzon, P. W. Halstenberg, T. Wang, X. Suo, S. Z. Yang, H. M. Meyer, Z. Wu, S. Dai, *J. Am. Chem. Soc.* **2021**, *143 (23)*, 8521–8526.
[15] J. C. Colmenares, A. Magdziarz, M. A. Aramendia, A. Marinas, J. M. Marinas, F. J. Urbano, J. A. Navio, *Catal. Commun.* **2011**, *16 (1)*, 1–6.
[16] D. Ramírez-Ortega, D. Guerrero-Araque, P. Acevedo-Peña, E. Reguera, H. A. Calderon, R. Zanella, *Int. J. Hydrogen Energy* **2021**, *46 (69)*, 34333–34343.
[17] F. Polo-Garzon, T. F. Blum, Z. Bao, K. Wang, V. Fung, Z. Huang, E. E. Bickel, D. E. Jiang, M. Chi, Z. Wu, *ACS Catal.* **2021**, *11 (4)*, 1938–1945.
[18] X. Pan, Y. J. Xu, *J. Phys. Chem. C* **2013**, *117 (35)*, 17996–18005.
[19] S. J. Tauster, S. C. Fung, R. L. Garten, *J. Am. Chem. Soc.* **1978**, *100 (1)*, 170–175.
[20] R. Wojcieszak, A. Jasik, S. Monteverdi, M. Ziolek, M. M. Bettahar, *J. Mol. Catal. A* **2006**, *256 (1–2)*, 225–233.
[21] R. Baker, *J. Catal.* **1983**, *79 (2)*, 348–358.
[22] A. Gonzalezelipe, *J. Catal.* **1982**, *76 (2)*, 254–264.
[23] N. Acerbi, S. C. Tsang, S. Golunski, P. Collier, *Chem. Commun.* **2008**, *13*, 1578.
[24] V. A. De la Peña O'Shea, M. Consuelo Álvarez Galván, A. E. Platero Prats, J. M. Campos-Martin, J. L. G. Fierro, *Chem. Commun.* **2011**, *47 (25)*, 7131.
[25] X. Liu, M. H. Liu, Y. C. Luo, C. Y. Mou, S. D. Lin, H. Cheng, J. M. Chen, J. F. Lee, T. S. Lin, *J. Am. Chem. Soc.* **2012**, *134 (24)*, 10251–10258.
[26] G. N. Vayssilov, Y. Lykhach, A. Migani, T. Staudt, G. P. Petrova, N. Tsud, T. Skála, A. Bruix, F. Illas, K. C. Prince, V. Matolı'n, K. M. Neyman, J. Libuda, *Nat. Mater.* **2011**, *10 (4)*, 310–315;'n, K. M. Neyman, J. Libuda, *Nat. Mater.* **2011**, *10 (4)*, 310–315.
[27] J. Silvestre-Albero, *J. Catal.* **2002**, *210 (1)*, 127–136.
[28] R. Baker, *J. Catal.* **1979**, *56 (3)*, 390–406.
[29] S. J. Tauster, S. C. Fung, R. T. K. Baker, J. A. Horsley, *Science* **1981**, *211 (4487)*, 1121–1125.
[30] S. J. Tauster, *Acc. Chem. Res.* **1987**, *20 (11)*, 389–394.
[31] P. Chen, A. Khetan, F. Yang, V. Migunov, P. Weide, S. P. Stürmer, P. Guo, K. Kähler, W. Xia, J. Mayer, H. Pitsch, U. Simon, M. Muhler, *ACS Catal.* **2017**, *7 (2)*, 1197–1206.
[32] J. H. Den Otter, H. Yoshida, C. Ledesma, D. Chen, K. P. De Jong, *J. Catal.* **2016**, *340*, 270–275.
[33] L. Y. Lin, S. Kavadiya, X. He, W. N. Wang, B. B. Karakocak, Y. C. Lin, M. Y. Berezin, P. Biswas, *Chem. Eng. J.* **2020**, *389*, 123450.
[34] Z. H. Qin, M. Lewandowski, Y. N. Sun, S. Shaikhutdinov, H. J. Freund, *J. Phys. Chem. C* **2008**, *112 (27)*, 10209–10213.
[35] D. N. Belton, Y. M. Sun, J. M. White, *J. Phys. Chem.* **1984**, *88 (9)*, 1690–1695.
[36] S. Neumann, H. H. Doebler, S. Keil, A. J. Erdt, C. Gutsche, H. Borchert, J. Kolny-Olesiak, J. Parisi, M. Bäumer, S. Kunz, *ACS Catal.* **2020**, *10 (7)*, 4136–4150.
[37] Z. H. Qin, M. Lewandowski, Y. N. Sun, S. Shaikhutdinov, H. J. Freund, *J. Phys. Chem. C* **2008**, *112 (27)*, 10209–10213.
[38] S. Liu, H. Qi, J. Zhou, W. Xu, Y. Niu, B. Zhang, Y. Zhao, W. Liu, Z. Ao, Z. Kuang, L. Li, M. Wang, J. Wang, *ACS Catal.* **2021**, *11 (10)*, 6081–6090.
[39] A. Lewera, L. Timperman, A. Roguska, N. Alonso-Vante, *J. Phys. Chem. C* **2011**, *115* (41), 20153–20159.
[40] J. Park, S. Lee, H. Kim, A. Cho, S. Kim, Y. Ye, J. W. Han, H. Lee, J. H. Jang, J. Lee, *Angew. Chem. Int. Ed.* **2019**, *58 (45)*, 16038–16042.
[41] F. Zhang, R. A. Gutiérrez, P. G. Lustemberg, Z. Liu, N. Rui, T. Wu, P. J. Ramírez, W. Xu, H. Idriss, M. V. Ganduglia-Pirovano, S. D. Senanayake, J. A. Rodriguez, *ACS Catal.* **2021**, *11 (3)*, 1613–1623.
[42] M. Mao, H. Lv, Y. Li, Y. Yang, M. Zeng, N. Li, X. Zhao, *ACS Catal.* **2016**, *6 (1)*, 418–427.
[43] J. Zhu Chen, A. Talpade, G. A. Canning, P. R. Probus, F. H. Ribeiro, A. K. Datye, J. T. Miller, *Catal. Today* **2021**, *371*, 4–10.
[44] F. Pesty, H.-P. Steinrück, T. E. Madey, *Surf. Sci.* **1995**, *339 (1–2)*, 83–95.
[45] O. Dulub, W. Hebenstreit, U. Diebold, *Phys. Rev. Lett.* **2000**, *84 (16)*, 3646–3649.
[46] S. Gan, Y. Liang, D. R. Baer, A. W. Grant, *Surf. Sci.* **2001**, *475 (1–3)*, 159–170.
[47] H.-P. Steinrück, F. Pesty, L. Zhang, T. E. Madey, *Phys. Rev. B* **1995**, *51 (4)*, 2427–2439.
[48] F. Rieboldt, S. Helveg, R. Bechstein, L. Lammich, F. Besenbacher, J. V. Lauritsen, S. Wendt, *Phys. Chem. Chem. Phys.* **2014**, *16 (39)*, 21289–21299.
[49] F. Rieboldt, L. B. Vilhelmsen, S. Koust, J. V. Lauritsen, S. Helveg, L. Lammich, F. Besenbacher, B. Hammer, S. Wendt, *J. Chem. Phys.* **2014**, *141 (21)*, 214702.
[50] B. Han, Y. Guo, Y. Huang, W. Xi, J. Xu, J. Luo, H. Qi, Y. Ren, X. Liu, B. Qiao, T. Zhang, *Angew. Chem. Int. Ed.* **2020**, *59 (29)*, 11824–11829.
[51] Z. Wu, Y. Li, W. Huang, *J. Phys. Chem. Lett.* **2020**, *11 (12)*, 4603–4607.
[52] A. Migani, G. N. Vayssilov, S. T. Bromley, F. Illas, K. M. Neyman, *Chem. Commun.* **2010**, *46 (32)*, 5936.
[53] Q. Fu, T. Wagner, *Surf. Sci. Rep.* **2007**, *62 (11)*, 431–498.
[54] B. Mei, C. Wiktor, S. Turner, A. Pougin, G. Van Tendeloo, R. A Fischer, M. Muhler, J. Strunk, *ACS Catal.* **2013**, *3*, 3041–3049.
[55] J. Zhang, H. Wang, L. Wang, S. Ali, C. Wang, L. Wang, X. Meng, B. Li, D. S. Su, F. S. Xiao, *J. Am. Chem. Soc.* **2019**, *141 (7)*, 2975–2983.
[56] H. Tang, Y. Su, B. Zhang, A. F. Lee, M. A. Isaacs, K. Wilson, L. Li, Y. Ren, J. Huang, M. Haruta, B. Qiao, X. Liu, C. Jin, D. Su, J. Wang, T. Zhang, *Sci. Adv.* **2017**, *3 (10)*, 1–9.
[57] Q. Fu, J. Dong, H. Li, J. Xiao, B. Yang, B. Zhang, Y. Bai, T. Song, R. Zhang, L. Gao, J. Cai, H. Zhang, Z. Liu, X. Bao, *J. Am. Chem. Soc.* **2020**, *142 (40)*, 17167–17174.
[58] K. Fujiwara, Y. Deligiannakis, C. G. Skoutelis, S. E. Pratsinis, *Appl. Catal. B* **2014**, *154–155*, 9–15.
[59] S. Bernal, G. Blanco, J. J. Calvino, C. López-Cartes, J. A. Pérez-Omil, J. M. Gatica, O. Stephan, C. Colliex, *Catal. Lett.* **2001**, *76* (3), 131–137.
[60] S. Bernal, J. J. Calvino, M. A. Cauqui, J. M. Gatica, C. López Cartes, J. A. Pérez Omil, J. M. Pintado, *Catal. Today* **2003**, *77 (4)*, 385–406.
[61] Y. Zhang, J. Liu, K. Qian, A. Jia, D. Li, L. Shi, J. Hu, J. Zhu, W. Huang, *Angew. Chem. Int. Ed.* **2021**, *60 (21)*, 12074–12081.
[62] A. Beck, X. Huang, L. Artiglia, M. Zabilskiy, X. Wang, P. Rzepka, D. Palagin, M.-G. Willinger, J. A. Van Bokhoven, *Nat. Commun.* **2020**, *11 (1)*, 3220.
[63] E. W. Zhao, H. Zheng, K. Ludden, Y. Xin, H. E. Hagelin-Weaver, C. R. Bowers, *ACS Catal.* **2016**, *6 (2)*, 974–978.
[64] S. Liu, W. Xu, Y. Niu, B. Zhang, L. Zheng, W. Liu, L. Li, J. Wang, *Nat. Commun.* **2019**, *10 (1)*, 5790.
[65] P. Wu, S. Tan, J. Moon, Z. Yan, V. Fung, N. Li, S. Z. Yang, Y. Cheng, C. W. Abney, Z. Wu, A. Savara, A. M. Momen, D. Jiang, D. Su, H. Li, W. Zhu, S. Dai, H. Zhu, *Nat. Commun.* **2020**, *11 (1)*, 3042.
[66] X. Liu, Z. D. Hood, Q. Zheng, T. Jin, G. S. Foo, Z. Wu, C. Tian, Y. Guo, S. Dai, W. Zhan, H. Zhu, M. Chi, *Nano Energy* **2019**, *55*, 441–446.
[67] J. Li, Y. Lin, X. Pan, D. Miao, D. Ding, Y. Cui, J. Dong, X. Bao, *ACS Catal.* **2019**, *9 (7)*, 6342–6348.
[68] H. Tang, Y. Su, B. Zhang, A. F. Lee, M. A. Isaacs, K. Wilson, L. Li, Y. Ren, J. Huang, M. Haruta, *Sci. Adv.* **2017**, *3*, e1700231.

[69] S. Hoang, S. P. Berglund, N. T. Hahn, A. J. Bard, C. B. Mullins, *J. Am. Chem. Soc.* **2012**, *134 (8)*, 3659–3662.
[70] J. C. Matsubu, S. Zhang, L. DeRita, N. S. Marinkovic, J. G. Chen, G. W. Graham, X. Pan, P. Christopher, *Nat. Chem.* **2017**, *9*, 120.
[71] F. Polo-Garzon, T. F. Blum, V. Fung, Z. Bao, H. Chen, Z. Huang, S. M. Mahurin, S. Dai, M. Chi, Z. Wu, *ACS Catal.* **2020**, *10 (15)*, 8515–8523.
[72] D. R. Mullins, M. D. Robbins, J. Zhou, *Surf. Sci.* **2006**, *600 (7)*, 1547–1558.
[73] J. E. Sutton, S. H. Overbury, A. Beste, *J. Phys. Chem. C* **2016**, *120 (13)*, 7241–7247.
[74] K. S. Kim, M. A. Barteau, W. E. Farneth, *Langmuir* **1988**, *4 (3)*, 533–543.
[75] J. Zhang, D. Zhu, J. Yan, C.-A. Wang, *Nat. Commun.* **2021**, *12 (1)*, 6665.
[76] H. Tang, F. Liu, J. Wei, B. Qiao, K. Zhao, Y. Su, C. Jin, L. Li, J. (Jimmy) Liu, J. Wang, T. Zhang, *Angew. Chem. Int. Ed.* **2016**, *55 (36)*, 10606–10611.
[77] G. D. Gesesse, C. Wang, B. K. Chang, S. H. Tai, P. Beaunier, R. Wojcieszak, H. Remita, C. Colbeau-Justin, M. N. Ghazzal, *Nanoscale* **2020**, *12 (13)*, 7011–7023.
[78] G. D. Gesesse, T. Le Neel, Z. Cui, G. Bachelier, H. Remita, C. Colbeau-Justin, M. N. Ghazzal, *Nanoscale* **2018**, *10* (43), 20140–20146.
[79] C. P. Ferraz, S. Navarro-Jaén, L. M. Rossi, F. Dumeignil, M. N. Ghazzal, R. Wojcieszak, *Green Chem.* **2021**, *23 (21)*, 8453–8457.
[80] J. L. Do, T. Friščić, *ACS Cent. Sci.* **2017**, *3 (1)*, 13–19.
[81] J. Zhang, J. Ma, T. S. Choksi, D. Zhou, S. Han, Y. F. Liao, H. Bin Yang, D. Liu, Z. Zeng, W. Liu, X. Sun, T. Zhang, B. Liu, *J. Am. Chem. Soc.* **2022**, *144 (5)*, 2255–2263.
[82] M. Li, T. Zhang, S. Z. Yang, Y. Sun, J. Zhang, F. Polo-Garzon, K. M. Siniard, X. Yu, Z. Wu, D. M. Driscoll, A. S. Ivanov, H. Chen, Z. Yang, S. Dai, *ACS Catal.* **2023**, *13 (9)*, 6114–6125.
[83] H. Pan, X. Wang, Z. Xiong, M. Sun, M. Murugananthan, Y. Zhang, *Environ. Res.* **2021**, *198*, 111176.
[84] R. Belgamwar, R. Verma, T. Das, S. Chakraborty, P. Sarawade, V. Polshettiwar, *J. Am. Chem. Soc.* **2023**, *145 (15)*, 8634–8646.
[85] Q. Fu, T. Wagner, S. Olliges, H. D. Carstanjen, *J. Phys. Chem. B* **2005**, *109*, 944.
[86] P. A. Anderson, *Phys. Rev.* **1949**, *76* (3), 388–390.
[87] H. K. Kim, A. S. Hyla, P. Winget, H. Li, C. M. Wyss, A. J. Jordan, F. A. Larrain, J. P. Sadighi, C. Fuentes-Hernandez, B. Kippelen, J. L. Brédas, S. Barlow, S. R. Marder, *Chem. Mater.* **2017**, *29 (8)*, 3403–3411.

Manuscript received: July 7, 2023
Revised manuscript received: September 5, 2023
Accepted manuscript online: September 7, 2023
Version of record online: ■■, ■■

REVIEW

This review focuses on recent efforts to enhance photocatalytic activities of metal nanoparticle-mediated photocatalysts through "strong metal-support interaction" (SMSI). Herein, we discuss the fundamentals of "strong metal-support interaction" and the methodology to practice the concept, involving synthesis and characterization techniques. The strengths and limitations of SMSI are also discussed, thus outlining future perspectives.

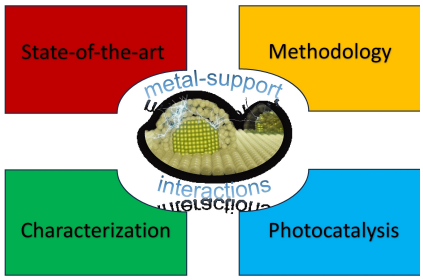

*Mr. V.-D. Quach, Dr. R. Wojcieszak, Dr. M. N. Ghazzal**